# TUDelft

Faculty of Industrial
Design Engineering

# Compatibility in Microstructural Topology Optimization

## A Physical Method for Generating Connectable Microstructures

MASTER THESIS

## Eric Garner

Delft University of Technology
MSc Integrated Product Design

August 3, 2018

Chair
Dr. ir. Jun Wu

Mentor
Prof. dr. Amir A. Zadpoor

DELFT UNIVERSITY OF TECHNOLOGY
DEPARTMENT OF DESIGN ENGINEERING

The undersigned hereby certify that they have read and recommend to the faculty
of Industrial Design Engineering for acceptance a thesis entitled

COMPATIBILITY IN MICROSTRUCTURAL TOPOLOGY OPTIMIZATION
A PHYSICAL METHOD FOR GENERATING
CONNECTABLE MICROSTRUCTURES

by

ERIC GARNER

in partial fulfillment of the requirements for the degree of

MASTER OF SCIENCE INTEGRATED PRODUCT DESIGN

Dated: <u>August 3, 2018</u>

Chair
_____
Dr. ir. J. Wu

Mentor
_____
Prof. dr. A. A. Zadpoor

# Abstract

Microstructural materials with spatially-varying properties, such as trabecular bone tissue, are widely seen in nature. These functionally graded structures possess smoothly changing microscale topologies that enable performance far superior to that of their base material. While the optimization of periodic microstructures has been studied in depth, less attention has been paid to the assembly of optimized microstructures with spatially varying properties. Existing works address this problem by ensuring geometric connectivity between adjacent microstructural unit cells. In this report, we argue that geometric connectivity is insufficient to ensure the continuation of physical properties, and propose the concept of mechanical compatibility. Mechanical compatibility directly examines the effective mechanical properties of the individual cell together with its neighbour. Our approach simultaneously optimizes the mechanical properties of individual microstructures as well as those of neighbouring pairs, so that material connectivity and smoothly varying physical properties are ensured. We demonstrate the application of our method in the design of functionally graded material for implant design, and in the design of both coupled and decoupled multiscale structures.

# Acknowledgements

Firstly, I would like express my sincere gratitude to Professor Jun Wu for introducing me to the field of topology optimization, and for his continuous support throughout this project. I would also like to thank Professor Amir Zadpoor and Eline Kolken for their helpful advice and constructive criticism. Finally, I have to thank Thomas and the whole staff and Cafe @Home for letting me work on my laptop all day and putting up with my terrible jokes.

# Contents

# List of Figures

# List of Abreviations

| | |
|---|---|
| **FEM** | Finite Element Method |
| **SIMP** | Simplified Isotropic Material with Penalization |
| **OC** | Optimality Criteria |
| **MP** | Mathematical Programming |
| **NLOPT** | Non-linear Optimization |
| **MMA** | Method of Moving Asymptotes |
| **FGM** | Functionally Graded Material |
| **PBC** | Periodic Base Cell |
| **GBC** | Global Base Cell |
| **CBC** | Compound Base Cell |
| **FDM** | Fused Deposition Modeling |
| **DIW** | Direct Ink Writing |
| **SLM** | Selective Laser Melting |
| **GF** | Global Filtering |

# 1 | Introduction

Topology optimization is a field at the intersection of mechanics, mathematics and physics which is concerned with finding the optimal spatial distribution of material, given a specific set of performance objectives and constraints (Bendsoe and Sigmund, 2011). As an example, Fig.1.1 shows a simply supported beam designed to be as stiff and as lightweight as possible when subjected to a load at its centre. This efficient use of material makes topology optimization a valuable design tool, particularly in aerospace and automotive applications, where weight minimization is key (Mot, 2006).
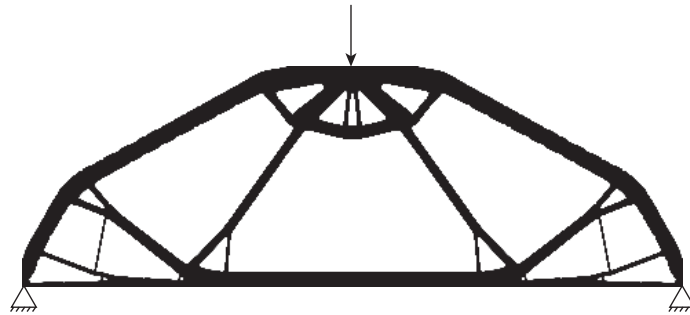
Figure 1.1: Typical structure generated using topology optimization.

Beyond finding the optimal distribution of traditional engineering materials, topology optimization can be used to develop new materials that are defined not only by their chemical composition, but by their microscopic structure. These so-called *metamaterials* can be designed to have highly tailored or extreme properties that are rare or even non-existent in nature (Sigmund, 2009). Examples of metamaterials designed to be as strong as possible under normal and shear loads are shown in Fig.1.2.
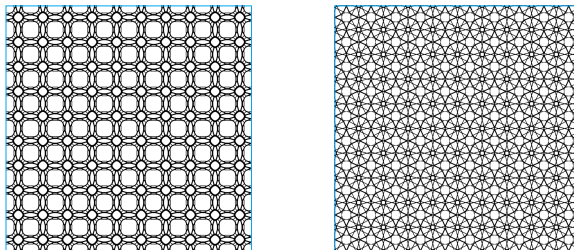
Figure 1.2: 2D metamaterials designed for maximum bulk modulus (left) and maximum shear modulus (right)

Their highly configurable nature makes metamaterials suitable for a wide range of applications, particularly in the design of biomedical devices, which must possess a high degree of mechanical compatibility with organic materials such as bone tissue (Kolken et al., 2018). Amazingly, if one looks closely at such organic materials, it appears that nature has also produced microstructures. The femoral cross-section in Fig.3.6 reveals an intricate structure which has been naturally optimized to balance the need for high strength and sufficient porosity for continuous bone regeneration.
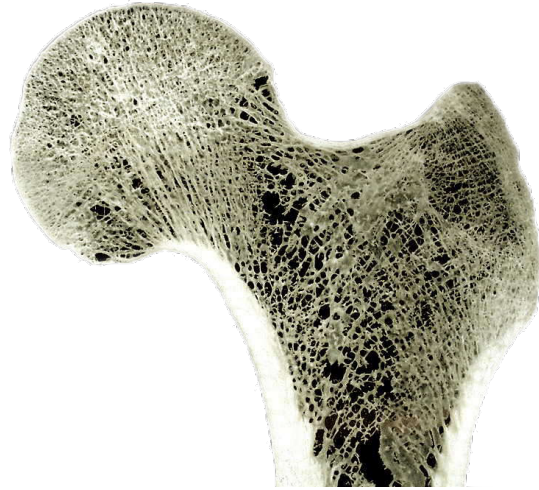


Figure 1.3: Femoral cross-section. Image retrieved from *digitalfolien.de* (2002)

It is often desirable to create metamaterials with spatially varying properties, like those which occur naturally in bone tissue. In practice, however, it is difficult to ensure physical compatibility between neighbouring microstructures. This can lead to unpredictable mechanical behaviour and unmanufacturable topologies. Fig.1.4 shows adjacent microstructures which exhibit exceptionally poor connection.

In recent years, several methods have been proposed to ensure geometric connectivity between adjacent microstructural unit cells. In this report, we argue that geometric connectivity is insufficient to ensure the continuation of physical properties, and propose the concept of mechanical compatibility. Mechanical compatibility directly examines the effective mechanical properties of the individual cell together with its neighbour. Our approach simultaneously optimizes the mechanical properties of individual microstructures as well as those of neighbouring pairs, so that material connectivity and smoothly varying physical properties are ensured.

## 1.1  Purpose of research and thesis outline

The overall aim of this research is to develop a generalized method for ensuring structural compatibility between adjacent microstructures in the design of materials with spatially varying mechanical properties. This is an essential step in the design of physically realizable functionally graded materials and multiscale structures.

The specific objectives of the proposed project are as follows:

1. Develop a material design algorithm which ensures physical compatibility between adjacent microstructures.

2. Apply the formulation to the design of materials with multi-dimensional functional gradation.
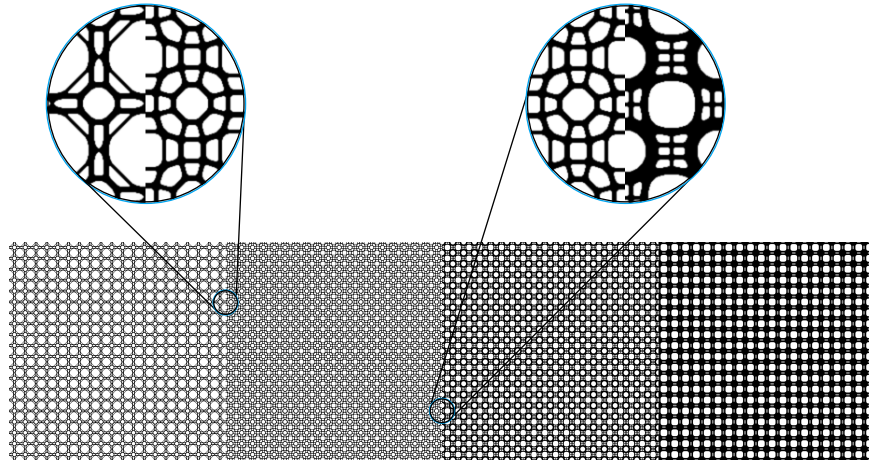
Figure 1.4: Functionally graded microstructural material designed for maximum bulk modulus, subject to linearly varying volume constraint from 30% to 60% (left to right).

3. Apply the formulation to decoupled multiscale topology optimization.

4. Apply the formulation to concurrent multiscale topology optimization.

5. Implement state-of-the-art length scale control techniques to material design

6. Evaluate the performance of the compatibility method and provide qualitative comparison with existing approaches.

## 1.2 Report structure

**Chapter 1** introduces the purpose of our research and presents the structure of this report.

**Chapter 2** presents an overview of topology optimization theory, methods and applications.

**Chapter 3** is a review of elasticity theory, homogenization theory and material design.

**Chapter 4** introduces the concept of multiscale structural design and presents decoupled and concurrent design algorithms.

**Chapter 5** presents the connectivity issue inherent to microstructural material design with inhomogeneous spatial distributions, and reviews existing approaches to address the issue.

**Chapter 6** presents a new compound cell formulation which addresses the connectivity issue by considering the physical behaviour of compound microstructures.

In **Chapter 7,** the compound formulation is applied to the design of multiscale structures.

In **Chapter 8**, several state-of-the-art feature length scale methods are applied to material design in an effort to reduce the manufacturing complexity inherent to functionally graded and multiscale structures.

**Chapter 9** presents physically realizable design examples generated using the compound formulation.

In **Chapter 10**, we evaluate the performance of the compound formulation by comparing theoretical results to full resolution FEM studies.

In **Chapter 11**, we present our conclusions and recommendations for further development.

# Part I

# Background

# 2 | Topology optimization

In this chapter, we present an overview of topology optimization and its use in material design. The theoretical background and mathematical formulation are first presented, followed by a review of elasticity and homogenization theory. Finally, topology optimization methods are applied to the design of tailored materials.

## 2.1 Structural optimization

Structural optimization is a class of problems concerned with finding the optimal layout of material, given a specific set of performance objectives and constraints. There are three general approaches to structural optimization: *sizing, shape* and *topology* optimization; the differences lie in how the design variables are defined.

In *sizing* problems, a ground structure is predefined, and the optimization objective is to find the optimal sizes of the different features within the ground structure. While this method guarantees structurally feasible results, it fundamentally limits the design space, resulting in optimized structures that are in fact far from optimal.

In *shape* optimization problems, the size and shape of structural features are not defined a priori. This allows for a wider solution space, producing results that generally outperform those achieved via size optimization.

*Topology* optimization is the most comprehensive optimization strategy in that the location, shape and size of all features are a function of the design variables. This results the widest possible design space, allowing for truly optimal designs (Sigmund, 2009). The three structural optimization categories are illustrated in Fig.2.1.

## 2.2 Problem formulation

All structural design problems can be described by a set of objectives, constraints and design variables. The general formulation is as follows: "Minimize (or maximize) an objective function subject to a set of constraints." A classic optimization problem is to maximize the stiffness of a structure, given a limited amount of material. More complicated problems may consider advanced mechanics, multi-physics, or problems with multiple objectives and constraints. In topology optimization problems, the design variables are typically the material density values throughout the design domain; they can be defined as either continuous or discrete.
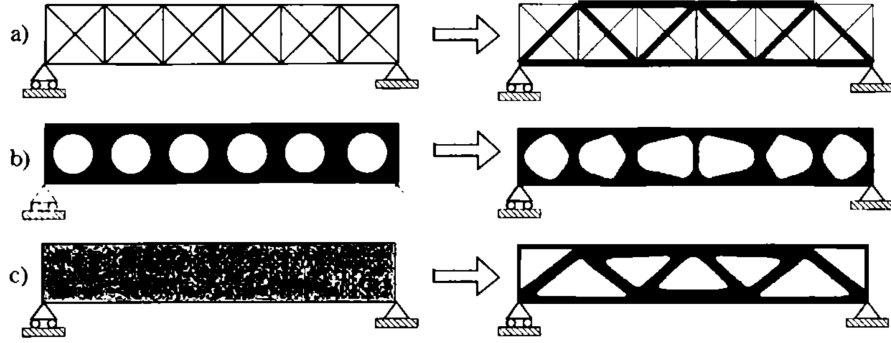
Figure 2.1: Categories of structural optimization. A) Sizing optimization of a truss structure, b) shape optimization and c) topology optimization. The initial problems are shown on the left and the optimized results are shown on the right. *(From Bendsøe and Sigmund, 2002, page 2)*

The general topology optimization problem can be formulated as follows (Sigmund and Maute, 2013): Consider a material design domain $\Omega$ in $\mathbb{R}^2$ or $\mathbb{R}^3$ that has been chosen so as to allow for the definition of all relevant loads and boundary conditions. The design domain $\Omega$ is first discretized into finite elements. The optimization objective is then to find the material distribution $\Omega^{mat}$ which minimizes a function $F$, typically subject to a volume constraint $G_0 \leq 0$ and possibly $M$ other constraints $G_i \leq 0, i = 1 \ldots M$. The material distribution is described by the density variable $\rho(x)$ which, in general, can take only the value 0 (void) or 1 (solid material) at every point $x$ in the design domain $\Omega$. In mathematical form:

$$
\begin{aligned}
\min_{\rho} \quad & F = F(\mathbf{u}(\boldsymbol{\rho}), \boldsymbol{\rho}) = \sum_i \int_{\Omega_i} f(\mathbf{u}(\rho_i), \rho_i) dV \\
\text{s.t.} \quad & : G_0(\boldsymbol{\rho}) = \sum_i v_i \rho_i - V_0 \leq 0 \\
& : G_j(\mathbf{u}(\boldsymbol{\rho}), \boldsymbol{\rho}) \leq 0, j = 1, \ldots, M \\
& : 0 \leq \rho_i \leq 1, i = 1, \ldots, N
\end{aligned}
\tag{2.1}
$$

where the state field $\mathbf{u}$ satisfies a linear or non-linear state equation.

## 2.2.1 Minimum compliance design

Considering the problem setup described above, the classic topology optimization problem aims to find the stiffest possible structure given a specific set of loading conditions and a limited amount of material. This is done by minimizing a characteristic property called the *compliance*, the inverse of the stiffness. An example setup and solution is shown in Fig.2.2.
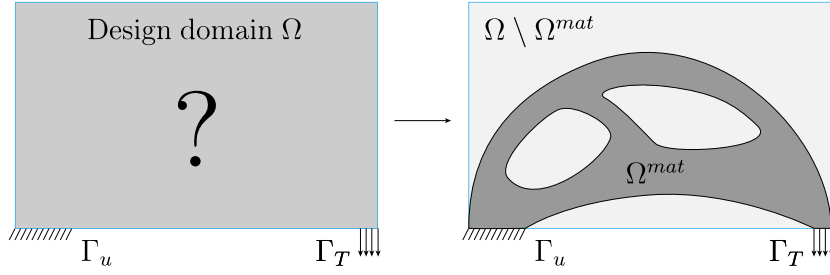
Figure 2.2: Illustration of a structural topology optimization problem.

Following the derivation from Bendsøe and Kikuchi (1988), we make use of the energy bilinear form, which is an expression of the internal virtual work in an elastic body at equilibrium $u$ for an arbitrary virtual displacement $v$:

$$a(u,v) = \int_\Omega E_{ijkl}(x)\epsilon_{ij}(u)\epsilon_{kl}(v)d\Omega \tag{2.2}$$

with linearized strains $\epsilon_{ij}(u) = \frac{1}{2}\left(\frac{\partial u_i}{\partial x_j} + \frac{\partial u_j}{\partial x_i}\right)$ and the load linear form

$$l(u) = \int_\Omega fud\Omega + \int_{\Gamma_T} tuds \tag{2.3}$$

where $U$ denotes the space of admissible displacement fields, $\Gamma_T$ is the boundary of $\Omega$, and $f$ and $t$ are body and boundary traction forces, respectively.

The minimum compliance problem can then be written as

$$
\begin{aligned}
\min_\rho \quad & l(u) \\
\text{s.t.} \quad & : a(u,v) = l(v), \text{for all } v \in U \\
& : E \in E_{ad}
\end{aligned}
\tag{2.4}
$$

When solving the problem by means of computational methods, it is convenient to express the problem in discretized form:

$$
\begin{aligned}
\min_\rho \quad & \mathbf{f}^T\mathbf{u} \\
\text{s.t.} \quad & : \mathbf{K}(E_e)\mathbf{u} = \mathbf{f} \\
& : E \in E_{ad}
\end{aligned}
\tag{2.5}
$$

Here, $\mathbf{u}$ and $\mathbf{f}$ are the global displacement and load vectors, respectively. $\mathbf{K}(E_e)$ is the global level stiffness matrix associated with element $e$.

The requirement that $E \in E_{ad}$ can be rewritten as:

$$E_{ijkl} = 1_{\Omega^{mat}} E_{ijkl}^0, \ 1_{\Omega^{mat}} = \begin{cases} 1 & \text{if } x \in \Omega^{mat} \\ 0 & \text{if } x \in \Omega \setminus \Omega^{mat} \end{cases}$$

$$\int_{\Omega} 1_{\Omega^{mat}} d\Omega = \text{vol}(\Omega^{mat}) \leq V \tag{2.6}$$

Finally, the problem can be written in a form suitable for numerical optimization

$$\begin{aligned} \min_{\rho} \quad & \mathbf{U}^T \mathbf{K} \mathbf{U} = \sum_{e=1}^{N} \mathbf{u}_e^T \mathbf{k}_e \mathbf{u}_e \\ \text{s.t.} \quad & : \mathbf{K} \mathbf{U} = \mathbf{F} \\ & : V(\mathbf{x})/V_0 = f \\ & : 0 \leq \rho \leq 1 \end{aligned} \tag{2.7}$$

where $\rho$ is the density vector (i.e. element densities), $N$ is the number of elements in the discretized design space, $V(\mathbf{x})$ and $V_0$ are the total material volume and design domain volume, respectively, and $f$ is a prescribed volume fraction. Note that upper case variables refer to the global level and lower case variables are the corresponding element level variables.

## 2.3  Optimization approaches

Since its introduction by Bensøe and Kikuchi in 1988, several approaches have been developed to tackle the topology optimization problem. The following section presents a brief overview of these approaches. Refer to Sigmund and Maute (2013), for a comprehensive review.

Generally speaking, topology optimization problems can be tackled by either a Lagrangian or an Eulerian approach. In the former, the problem is converted into a shape optimization problem by introducing a mesh which follows the shape boundaries. In the later, a fixed mesh is defined and the element density values are the design variables. This section focusses on the most common Eulerian method, generally referred to as the density approach.

## 2.3.1 Material interpolation

The density approach involves discretization of the design domain $\Omega$ into $N$ finite elements, and letting the density distribution $\boldsymbol{\rho}(x)$ be described either by element or nodal variables. In general, the density $\boldsymbol{\rho}(x)$ must be either 0 or 1 at any position $x$ on $\Omega$. However, strict application of this requirement may cause the problem to lack solution. Instead, a relaxed formulation is often employed. These formulations introduce a continuous density variable over the 0-1 domain. The material properties are then interpolated from the density via a smooth interpolation function. This allows for the use of gradient-based optimization algorithms and ensures reasonably rapid convergence.

A simple and powerful interpolation scheme introduced by Bensøe (1989) is the so-called SIMP (Simplified Isotropic Material with Penalization) or power-law approach.

$$E(\rho_i) = \rho_i^{\gamma} E_0 \tag{2.8}$$

where $\gamma$ is a penalization parameter and $E_0$ is the Young's modulus of a solid element of base material. For $\gamma > 1$, this scheme penalizes intermediate values, as shown in Fig.2.3, and encourages convergence to a binary solution. An appropriate choice of $\gamma$ is necessary for full convergence to a global minimum.
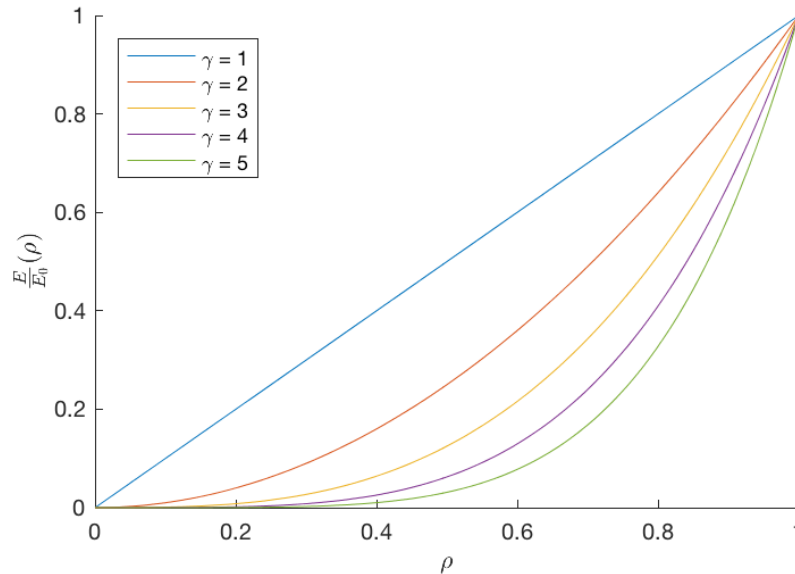


Figure 2.3: Normalized Young's modulus as a function of density for different penalization parameter values

Since the introduction of SIMP, a number of alternative schemes and modifications have been proposed. Among them is the so-called Modified SIMP approach, which helps alleviate the issue of residual intermediate values in the final solution:

$$E(\rho_i) = E_{min} + \rho_i^\gamma (E_0 - E_{min}) \tag{2.9}$$

where the additional $E_{min}$ term is an arbitrary small non-zero term that prevents the global stiffness matrix from becoming singular.

Assuming a fixed Poisson's ratio, the stiffness matrix of an element with intermediate density is:

$$K(\rho_i) = E(\rho_i) * k_0 \tag{2.10}$$

where $k_0$ is the stiffness matrix of a solid element of base material.

## 2.3.2 Filtering

In order to ensure mesh independency and avoid the common checkerboard problem, filtering techniques are usually employed, particularly when using low order elements. A mesh independency filter can be applied to the design variable sensitivities. It works by modifying each element's sensitivity to be a weighted average of its neighbours, within a prescribed radius $r_{min}$ (Sigmund, 2007):

$$\widehat{\frac{\partial c}{\partial x_i}} = \frac{\sum_{i \in \mathbb{M}} \omega_{i,e} \frac{\partial c_i}{\partial x_i}}{\sum_{i \in \mathbb{M}} \omega_{i,e}} \tag{2.11}$$

where $\mathbb{M}$ is the set of elements in the neighbourhood of element $e$, i.e.

$$\mathbb{M} = \{i | \|x_i - x_e\|_2 \le r_e\} \tag{2.12}$$

and $r_e$ is the filter radius. The weighting factor is defined linearly with respect to the distance between elements

$$\omega_{i,e} = 1 - \frac{\|x_i - x_e\|_2}{r_e} \tag{2.13}$$
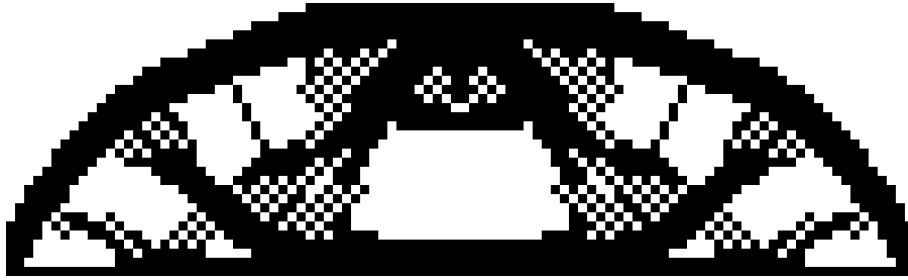


Figure 2.4: Optimization result of simply supported beam exhibiting checkerboard pattern

In addition to sensitivity filtering, a similar technique can be applied to the element densities. In this case, the filter produces a so-called physical density $\bar{\rho}$, which is a weighted average of the design variable in a neighbourhood of radius $r_{min}$.

$$\bar{\rho}_e = \frac{\sum_{i \in \mathbb{M}} \omega_{i,e} \rho_i}{\sum_{i \in \mathbb{M}} \omega_{i,e}} \tag{2.14}$$

An unfortunate side effect of mesh-independency filter is that it leaves an undesirable grey zone of width $r_{min}$ between the solid and void regions. This issue can be resolved by using a projection scheme. In general,

$$\tilde{\rho}_e(\bar{\rho}) = \begin{cases} 1 & \text{if } \bar{\rho} \geq \frac{1}{2}, \\ 0 & \text{otherwise} \end{cases}$$

However, for this type of numerical optimization, a relaxation method must be used. The non-differentiable function can be approximated by

$$\tilde{\rho}_e(\bar{\rho}) = \frac{\tanh(\frac{\beta}{2}) + \tanh(\beta(\bar{\rho} - \frac{1}{2}))}{2 \tanh(\frac{\beta}{2})} \tag{2.15}$$

where $\beta$ controls the sharpness of the transition as illustrated in Fig.2.5, and is progressively increased over the course of the optimization to avoid instability (Wang et al., 2011).
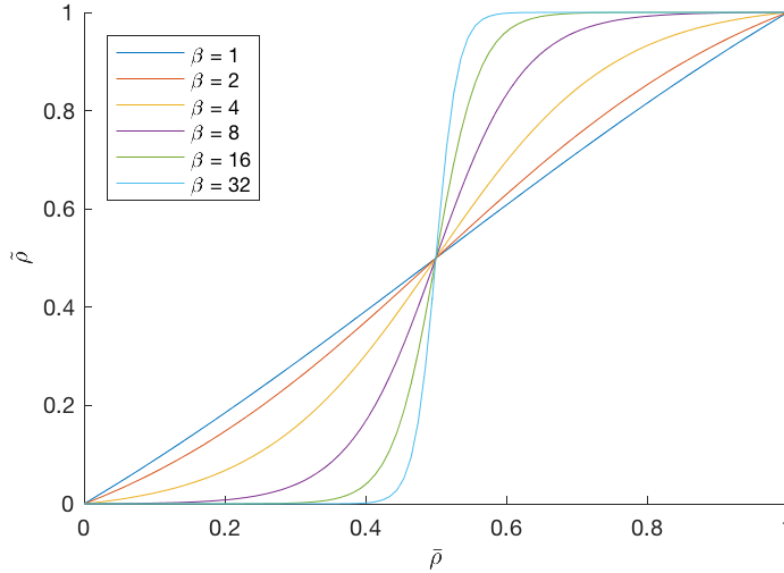


Figure 2.5: Projection function for various values of $\beta$. As $\beta$ increases, the function approximates the original unit step function.

### 2.3.3 Numerical solution

Due to the inherently non-linear nature of topology optimization problems, the use of numerical methods is unavoidable. Solutions are found via an iterative procedure through which the design variables are updated according to the current state of the system. The two most common procedures are the optimality criteria method and mathematical programming. Fig.2.6 shows the general structural optimization procedure.
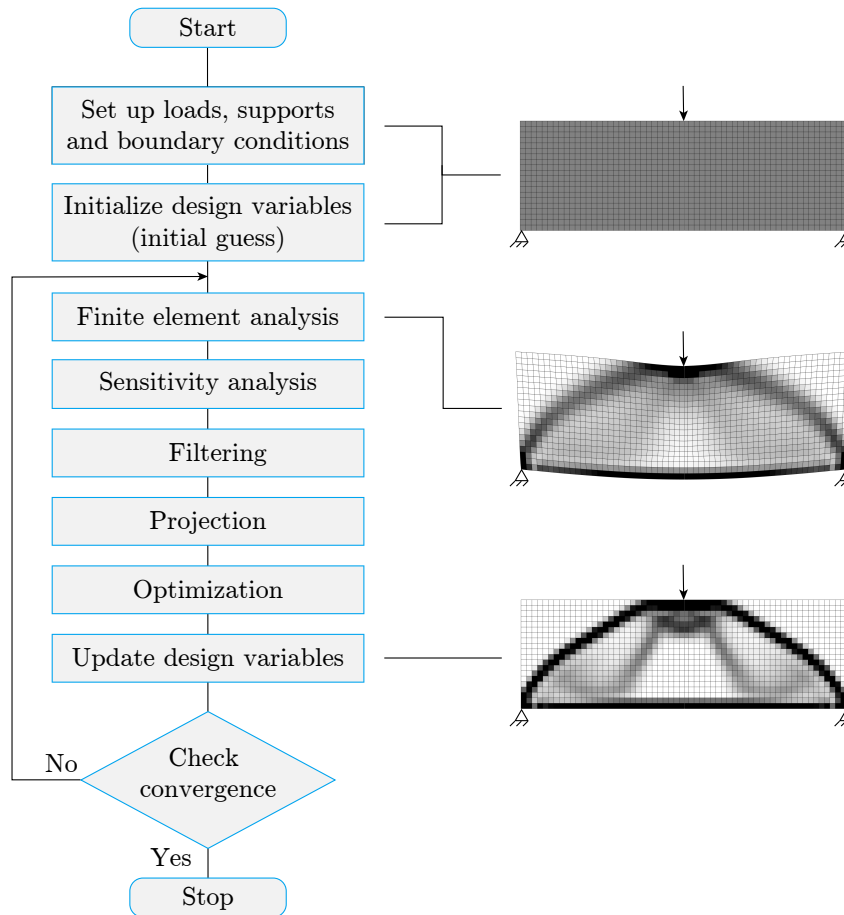


Figure 2.6: Structure of typical structural topology optimization procedure.

## Optimality criteria

The optimality criteria method (OC) is a variant of the Lagrange multiplier approach, which has been adapted for problems with a large number of design variables subject to a small number of constraints (Patnaik et al., 1995). The Lagrange multiplier approach combines the objective $f$ and constraints $g_j$ into a single energy functional

$$\mathcal{L}(\mathbf{x}, \boldsymbol{\lambda}) = f(\mathbf{x}) + \sum \lambda_j \nabla g_j^*(\mathbf{x}) \tag{2.16}$$

The unknown vectors $\mathbf{x}$ and $\boldsymbol{\lambda}$ are found from the stationary conditions of the Lagrangian $\mathcal{L}(\mathbf{x}, \boldsymbol{\lambda})$. In the OC method, the stationary conditions of the Lagrangian are used to develop a set of rules which guide the iterative update of the design variables. Though extremely efficient, the OC method has one major limitation: it is generally only suitable for single constraint problems.

## Mathematical programming

Mathematical programming (MP) algorithms such as NLOPT and MMA (Svanberg, 1987) are popular alternatives to the OC method because of their ability to handle multiple constraints. They operate by updating the design variables base on the current state of the objective function and constraints, and their respective sensitivities.

# 3 | Material design

Before presenting the material design problem formulation, we briefly review Hooke's law for continuous media.

## 3.1 Hooke's law

Hooke's law states that the magnitude of a force $\mathbf{F}$ needed to extend or compress a spring by a distance $x$ is linearly proportional to $x$. The same linear relation applies to the behaviour of many materials under small elastic deformation. In Fig.3.1, a 2D isotropic material subject to a normal stress $\sigma_{11}$ in the $x$ direction undergoes strains $\varepsilon_{11}$ and $\varepsilon_{22}$, described by

$$\varepsilon_{11} = \frac{1}{E}\sigma_{11} \tag{3.1}$$

$$\varepsilon_{22} = \frac{-1}{E}\upsilon\sigma_{11} \tag{3.2}$$

where $\upsilon$ is the Poisson's ratio, which is an expression of the deformation in one direction due to an applied stress in a perpendicular direction.
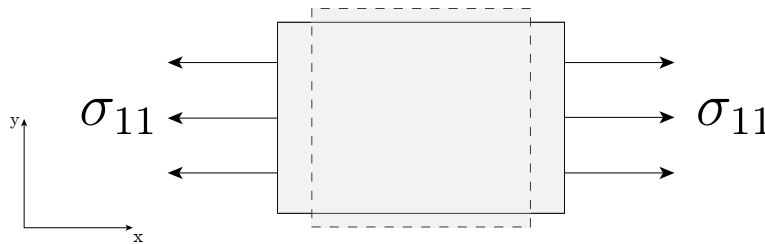


Figure 3.1: 2D material subjected to normal stress $\sigma_{11}$

When stresses are applied in both (2D) or all three (3D) directions, the resulting strains can be expressed as,

$$\varepsilon_{ij} = \frac{1}{E}[(1+\upsilon)\sigma_{ij} - \upsilon\delta_{ij}\sigma_{kk}] \tag{3.3}$$

which, when inverted, yields a more useful expression of stress as a function of strain

$$\sigma_{ij} = \frac{E}{(1+\upsilon)}\left[\varepsilon_{ij} + \frac{\upsilon}{1-2\varepsilon}\delta_{ij}\varepsilon_{kk}\right] \tag{3.4}$$

The stiffness tensor is the derivative of the stress $\sigma_{ij}$ with respect to strain $\varepsilon_{kl}$.

$$C_{ijkl} = \frac{\partial \sigma_{ij}}{\partial \varepsilon_{kl}} = \frac{E}{(1+\upsilon)} \left[ \frac{1}{2}(\delta_{ik}\delta_{jl} + \delta_{jk}\delta_{il}) + \frac{\upsilon}{(1-2\upsilon)})\delta_{ij}\delta_{kl} \right] \tag{3.5}$$

This expression described the mechanical properties of any linearly elastic isotropic material.

The bulk modulus $\kappa$ is the ratio of hydrostatic stress $\sigma_{hyd}$ to volumetric strain. In other words, it is a measure of the compressibility of a material under uniform pressure. For an isotropic 2D material, the bulk modulus is given by

$$\kappa = \frac{\sigma_{hyd}}{\varepsilon_{vol}} = \frac{E}{3(1-2\upsilon)} = \frac{1}{4}(C_{1111} + C_{1122} + C_{2211} + C_{2222}) \tag{3.6}$$
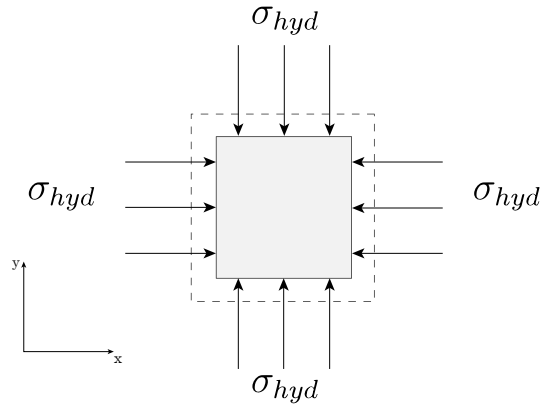


Figure 3.2: 2D material subjected to hydrostatic stress $\sigma_{hyd}$

The shear modulus $G$ is the resistance of a material to deform under the influence of a shear load. It is defined as the ratio of the shear stress $\tau_{12}$ over the shear strain $\gamma_{12}$:

$$G = \frac{\tau_{12}}{\gamma_{12}} = \frac{E}{2(1+\upsilon)} = C_{1212} \tag{3.7}$$
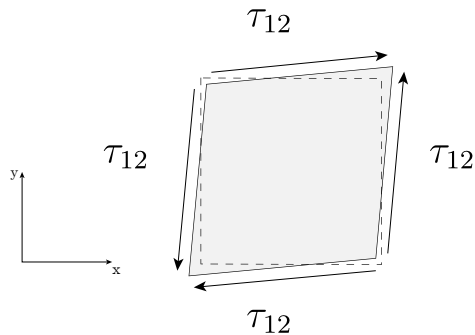


Figure 3.3: 2D material subjected to shear stress $\tau_{12}$

## 3.2 Homogenization

Topology optimization can be used in combination with homogenization theory to design materials with highly tailored or extreme properties that are rare or even non-existent in nature. The basic idea is that the mechanical properties of a heterogenous material composed of periodically repeating microscopic unit cells are defined not only by the base material but by the topology of the unit cell. The material design problem is that of finding the optimal unit cell topology, given a specific performance objective.

Consider a heterogeneous material composed of periodically repeating microscopic unit cells $Y$ in $\mathbb{R}^2$ or $\mathbb{R}^3$, as shown in Fig.3.4
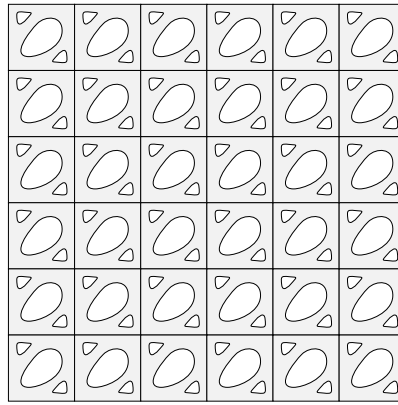


Figure 3.4: Periodic material composed of identical unit cells

The unit cell can be defined as

$$Y = ]0, y_1^0[\times]0, y_2^0[ \text{ in } \mathbb{R}^2, \text{ or}$$
$$Y = ]0, y_1^0[\times]0, y_2^0[\times]0, y_3^0[ \text{ in } \mathbb{R}^3 \tag{3.8}$$

where $y_1^0$, $y_2^0$ and $y_3^0$ are the dimensions of the base cell along the principle axes. Due to the periodicity, any physical characteristic $\mathcal{F}$ has the following property

$$\mathcal{F}(\mathbf{x} + \mathbf{N}\mathbf{Y}) = \mathcal{F}(\mathbf{x}) \tag{3.9}$$

where $\mathbf{x} = (x_1, x_2, x_3)$ is the position vector, $\mathbf{N}$ is a $3 \times 3$ diagonal matrix

$$\mathbf{N} = \begin{bmatrix} n_1 & 0 & 0 \\ 0 & n_2 & 0 \\ 0 & 0 & n_3 \end{bmatrix},$$

where $n_1$, $n_2$ and $n_3$ are arbitrary integers and $\mathbf{Y} = \langle Y_1, Y_2, Y_3 \rangle^T$ is a constant vector which determines the period in each of the principle directions.

In other words, the characteristic properties of the heterogenous medium are a function of two independent scales: the macroscopic *global* scale **x** and the microscopic *local* scale **y**. On the local scale, these characteristic functions may oscillate rapidly but on the global scale they behave smoothly, as shown in Fig.3.5. As long as the dimensions of the unit cell are very small compared to those of the macroscopic structure, and the geometry of the unit cell is either constant of slowly changing, only the global scale need be considered. Moreover, the effective properties of the heterogeneous medium can be obtained from the geometry of a single unit cell.
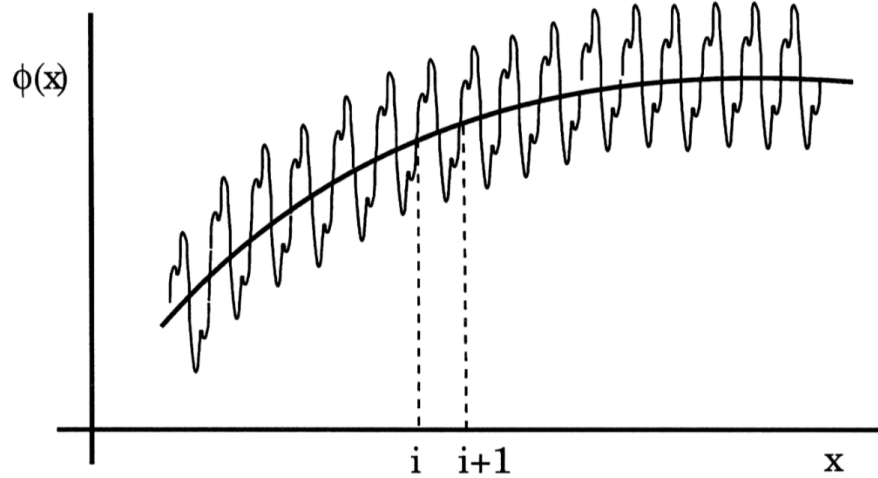


Figure 3.5: Function with high local oscillation and smooth global variation. *From Hassani and Hinton (1998)*

Characteristic functions of the heterogeneous medium can be expressed according to the double scale asymptotic expansion

$$\Phi^\epsilon(x) = \Phi^0(x, y) + \epsilon\Phi^1(x, y) + \epsilon^2\Phi^2(x, y) + \ldots, \qquad (3.10)$$

where $\epsilon = \frac{y}{x}$. Since $\epsilon$ is very small, only the first order terms of the expansion need to be considered.

## 3.3 Homogenization formulae for periodic composite structures

Applying these concepts, the homogenized stiffness tensor $\bar{C}_{ijkl}$ of any heterogeneous medium with periodically repeating microscale geometry is given by the average of the integral over the base cell $Y$ as

$$\bar{C}_{ijkl} = \frac{1}{|Y|} \int_Y C_{ijpq}(\varepsilon_{pq}^{0(kl)} - \varepsilon_{pq}^{*(kl)})dY \tag{3.11}$$

where $\varepsilon_{pq}^{*(kl)}$ is the Y-periodic solution of

$$\int_Y C_{ijpq}\varepsilon_{pq}^{*(kl)}\frac{\partial v_i}{\partial y_j}dY = \int_Y C_{ijpq}\varepsilon_{pq}^{0(kl)}\frac{\partial v_i}{\partial y_j}dY, \tag{3.12}$$

where $v$ is the Y-periodic admissible displacement field and $\varepsilon_{pq}^{0(kl)}$ correspond to three or six linearly independent unit test strains in 2D or 3D, respectively.

The effective elasticity matrix can also be written in terms of element mutual energies

$$\bar{C}_{ijkl} = \frac{1}{|Y|} \int_Y C_{pqrs}\varepsilon_{pq}^{A(ij)}\varepsilon_{rs}^{A(kl)}dY \tag{3.13}$$

In finite element form, for a base cell discretized into $N$ elements, the effective tensor is approximated by

$$\bar{C}_{ijkl} = \frac{1}{|Y|} \sum_{e=1}^{N}(\mathbf{u}_e^{A(ij)})\mathbf{k}_e\mathbf{u}_e^{A(kl)} \tag{3.14}$$

where $\mathbf{u}_e^{A(kl)}$ are the element displacement solutions corresponding to the unit test strain fields $\varepsilon^{0(kl)}$.

Each element of the homogenized elasticity tensor is the average of the element mutual energies, for the three unit test strains.. Using Voigt notation,

$$\bar{C}_{ij} = \frac{1}{|Y|} \sum_{i=1}^{N} q_e^{(ij)}, \ q_e^{ij} = (\mathbf{u}_e^{A(i)})^T\mathbf{k}_e\mathbf{u}_e^{A(j)} \tag{3.15}$$

This form is very similar to the objective function of the minimum compliance problem described in Section 2.2.1. In fact, the design of tailored materials can be performed in much the same way, with the addition of periodic boundary conditions.

## 3.4 Material design problem formulation

In the material design problem, the objective is to find the optimal topology of a single unit cell. The unit cell is first discretized into $N$ finite elements, each with a corresponding density variable $\rho(x)$. The elemental Young's moduli $E_e(\rho_e)$ are evaluated using the modified SIMP scheme described in Section 2.3.1. The global stiffness matrix $\mathbf{K}$ is then assembled and used to solve the equilibrium equation and evaluate the homogenized stiffness tensor $\bar{C}_{ijkl}$ of the structure.

The mathematical formulation, from Xia and Breitkopf (2015), is:

$$
\begin{aligned}
\min_{\rho} \quad & c\big(\bar{C}_{ijkl}(\rho)\big) \\
\text{s.t.} \quad & : \mathbf{K}\mathbf{U}^{A(kl)} = \mathbf{F}^{(kl)}, \ k,l = 1,\ldots,d \\
& : \frac{1}{|Y|}\sum_{e=1}^{N} v_e \rho_e \leq V_0 \\
& : 0 \leq \rho_e \leq 1, \, e = 1,\ldots,N
\end{aligned}
\tag{3.16}
$$

where $\mathbf{U}^A(kl)$ and $\mathbf{F}^{(kl)}$ are the global displacement and external force vectors for each of the unit test cases $(kl)$, respectively. $d$ is the spatial dimention, $v_e$ is the element volume, and $V_0$ is the prescribed maximum volume fraction. The objective function $c(\bar{C}_{ijkl}(\rho))$ is a function of the homogenized stiffness tensor, and can take different forms, depending on the desired mechanical properties. In the following, we formulate the objective functions for the two main material design problems: design for *extreme* properties and design for *tailored* properties.

The design of materials with extreme properties involves the minimization of some function of the homogenized stiffness tensor $\bar{C}_{ijkl}$. The objective take the form:

$$
c\big(\bar{C}_{ijkl}(\rho)\big) = \sum_{i,j=1}^{3} r_{ij}(\bar{C}_{ij})
\tag{3.17}
$$

where $r_{ij}$ is a function of $\bar{C}_{ij}$.

For example, the design of a 2D material with maximized bulk modulus corresponds to the minimization of

$$
c\big(\bar{C}_{ijkl}(\rho)\big) = -(C_{1111} + C_{1122} + C_{2211} + C_{2222})
\tag{3.18}
$$

Materials with tailored mechanical properties are obtained by minimizing the square of the difference between the desired and homogenized tensor values. In mathematical form, from Zhou and Li (2008),

$$
c\big(\bar{C}_{ijkl}(\rho)\big) = \sum_{i,j=1}^{3} r_{ij}(C_{ij}^{*} - \bar{C}_{ij})^2
\tag{3.19}
$$

where $C_{ij}^{*}$ is the desired stiffness tensor.

## 3.5 Functionally graded materials

Materials with spatially varying porous structures are widely seen in nature. They are the result of an organic optimization process which balances global structural performance requirements and local topological constraints (Wessel, 2004). Trabecular bone tissue, for example, possesses a highly heterogenous material distribution designed to be strong and lightweight, while maintaining sufficient porosity for continuous tissue regeneration. The synthetic design of such functionally graded materials (FGM) is the subject of this chapter.



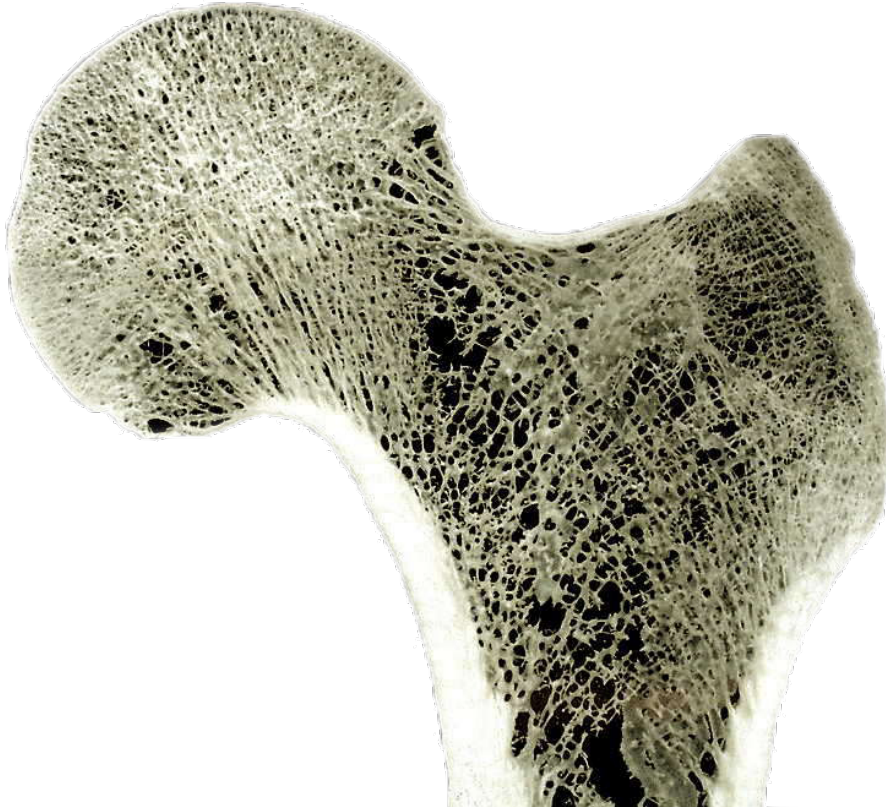Figure 3.6: Femoral cross-section. Image retrieved from *digitalfolien.de* (digitalfolien, 2002)

Consider the design of a 2D FGM with gradation in one direction and periodicity in the other, as shown in Fig.3.7. The typical FGM formulation minimizes the sum of the objective functions for each of the individual periodic base cells (PBC).
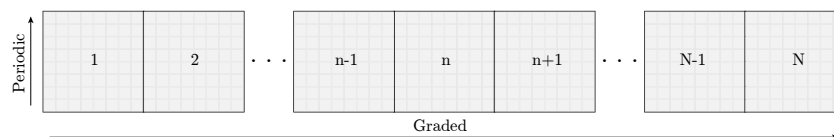


Figure 3.7: Global base cell comprised of $N$ periodic base cells.

In mathematical form, the design of functionally graded materials can be written as:

$$\min_{\rho} \quad \sum_{n=1}^{N} c_n(\bar{C}_{ij}^n(\boldsymbol{\rho}))$$

$$\text{s.t.} \quad : \mathbf{K}_n \mathbf{U}_n^{A(kl)} = \mathbf{F}_n^{(kl)}, \ k, l = 1, ..., d, \ n = 1, ..., N$$

$$: \sum_{e=1}^{M} v_e \rho_e / |Y_n| \leq V_n \ n = 1, ..., N \tag{3.20}$$

$$: 0 \leq \rho_e \leq 1, e = 1, ..., N \times M$$

where, for each unit cell $n$, $\mathbf{K}_n$ is the global stiffness matrix, $\mathbf{U}_n^{A(kl)}$ and $\mathbf{F}_n^{(kl)}$ are the global displacement vector and external force vector of the test case $(kl)$, respectively. FGM's can be optimized to possess either tailored or extreme local properties. Fig.3.8 shows an FGM optimized for maximum bulk modulus under linearly varying local volume constraint.
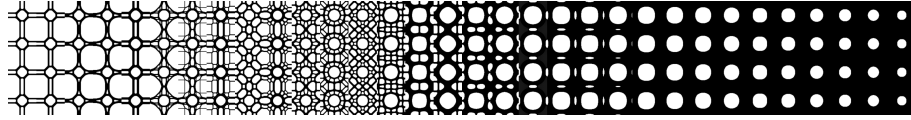


Figure 3.8: 2D FGM optimized for maximum bulk modulus with 1D linearly varying volume constraint from 20% to 90%.

The optimized properties of the individual PBC's are plotted in Fig.3.9, along with the Hashin-Shtrickman theoretical bounds for two-phase materials (Hashin and Shtrikman, 1963). It is apparent that the local material properties have indeed been maximized. However, when observing the boundaries between adjacent PBC's, there is often little, if any, material connectivity (see Fig.3.10). As a result, the FGM may not be manufacturable and will not perform as expected under load. The connectivity issue is the subject of Chapter 5.
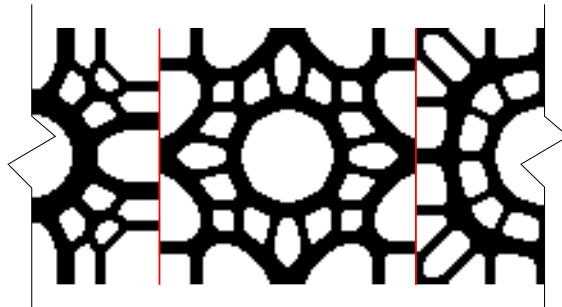


Figure 3.10: Material discontinuity between adjacent microstructures in FGM.
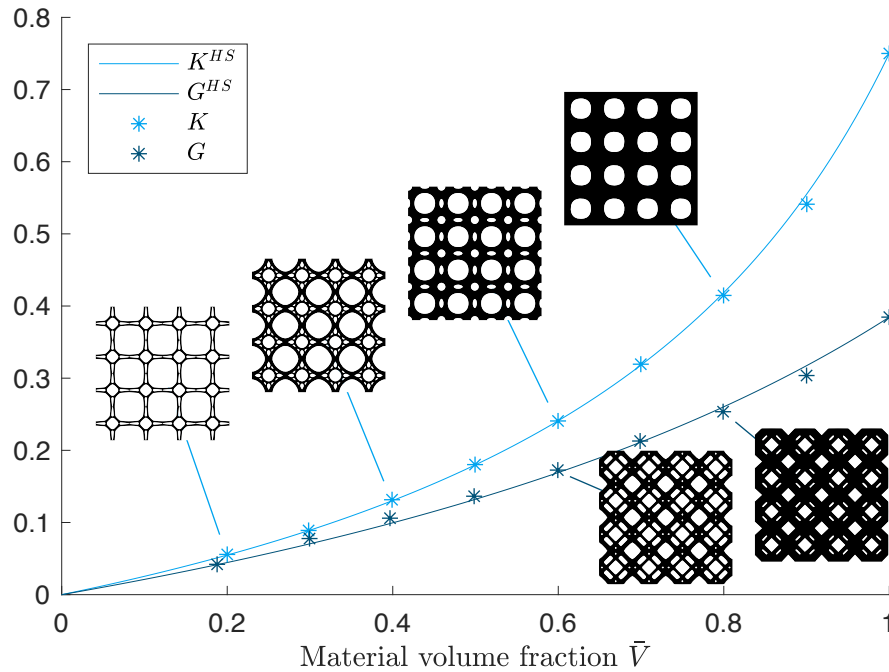
Figure 3.9: Maximized bulk and shear moduli as a function of average material density, along with corresponding Hashin-Shtrickman theoretical bounds

## 3.6 Summary

The design of functionally graded materials has a wide range applications, particularly in the field of biomechanical engineering, in which mechanical compatibility with organic tissue is of primary importance. The existing topology optimization-based approaches generally do not account for boundary conditions, which leads to material connectivity problems. As a result, the optimized structures are often unmanufacturable and do not perform as expected.

# 4 | Multiscale structural design

In addition to single scale structures or materials, topology optimization can be applied to the design of multiscale structures, which possess both optimized global scale material distribution and optimized local materials properties. An example of a multiscale simply supported beam is shown in Fig.4.1. In this chapter, we introduce two common approaches to the multiscale optimization problem: the *decoupled* bottom-up method, and the *concurrent* hierarchical free-material method.
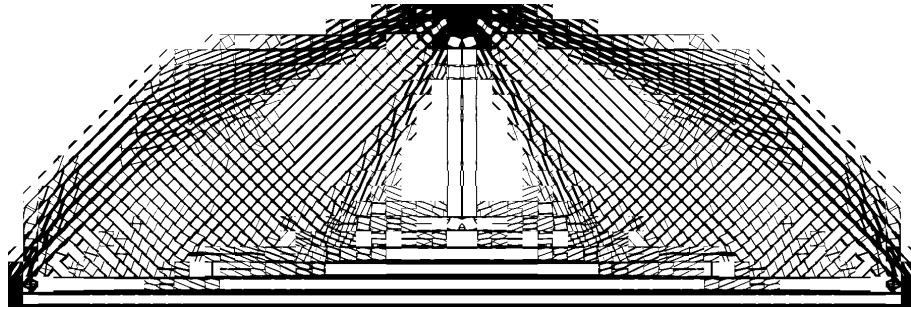


Figure 4.1: Simply supported beam generated via multiscale optimization with 30 by 30 micro unit cells and 30 by 20 macro unit cells.

## 4.1 Bottom-up multiscale optimization

A bottom-up approach was proposed by Cramer et al. (2016). In this method, a series of isotropic microstructures are optimized for maximum bulk modulus. The homogenized properties are then fitted to a functional with the form of the Hashin-Shtrickman bounds. The resulting smooth functions are then used to replace the traditional SIMP method in a single scale macro level optimization procedure. Fig.4.4 presents the procedure flow.

Isotropy can be ensured in the microstructure design process by imposing a cubic symmetry constraint and

$$\bar{C}_{11} + \bar{C}_{22} - (\bar{C}_{12} + \bar{C}_{21}) - 4\bar{C}_{33} = 0 \tag{4.1}$$
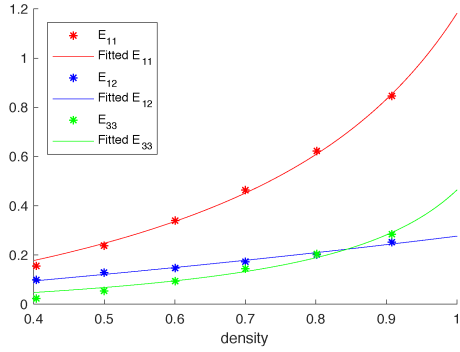
Figure 4.2: Fitted material property interpolation functions.
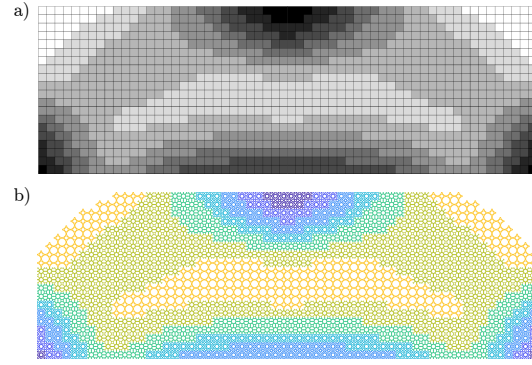


Figure 4.3: a) Non-binary material distribution; b) Equivalent multiscale material distribution

The isotropy constraint ensures that the interpolation functions closely match the homogenized elastic properties of the microstructures. Moreover, it reduces the number of parameters required to build the stiffness matrix from 6 (2D) or 21 (3D) to 2 (or 3 if slight anisotropy due to FEM discretization is taken into account). This significantly reduces the computational cost of the procedure, particularly for 3D implementations.

The fitting functional take the form:

$$\bar{C}_{ijkl}^{fit}(\rho) = \bar{C}_{ijkl}^{0}\left(1 - \frac{1-\rho}{1+a_{ijkl}\rho}\right) \tag{4.2}$$

The functional matches the data very closely, and has the appropriate boundary values, i.e., $\bar{C}_{ijkl}^{fit}(0) = 0$ and $\bar{C}_{ijkl}^{fit}(1) = C_{ijkl}^{0}$ (see Fig.4.2).

Since the interpolation functions are concave, bottom-up optimization procedures generally lead to binary solutions in which no microstructures are present. However, in the case of non-convergent single scale optimization problems, this method allows for the physical realization of greyscale elements. Fig.4.3 shows an example of a greyscale material distribution replaced with equivalent black and white microstructures. The microstructures are shown in colour for illustrative purposes.
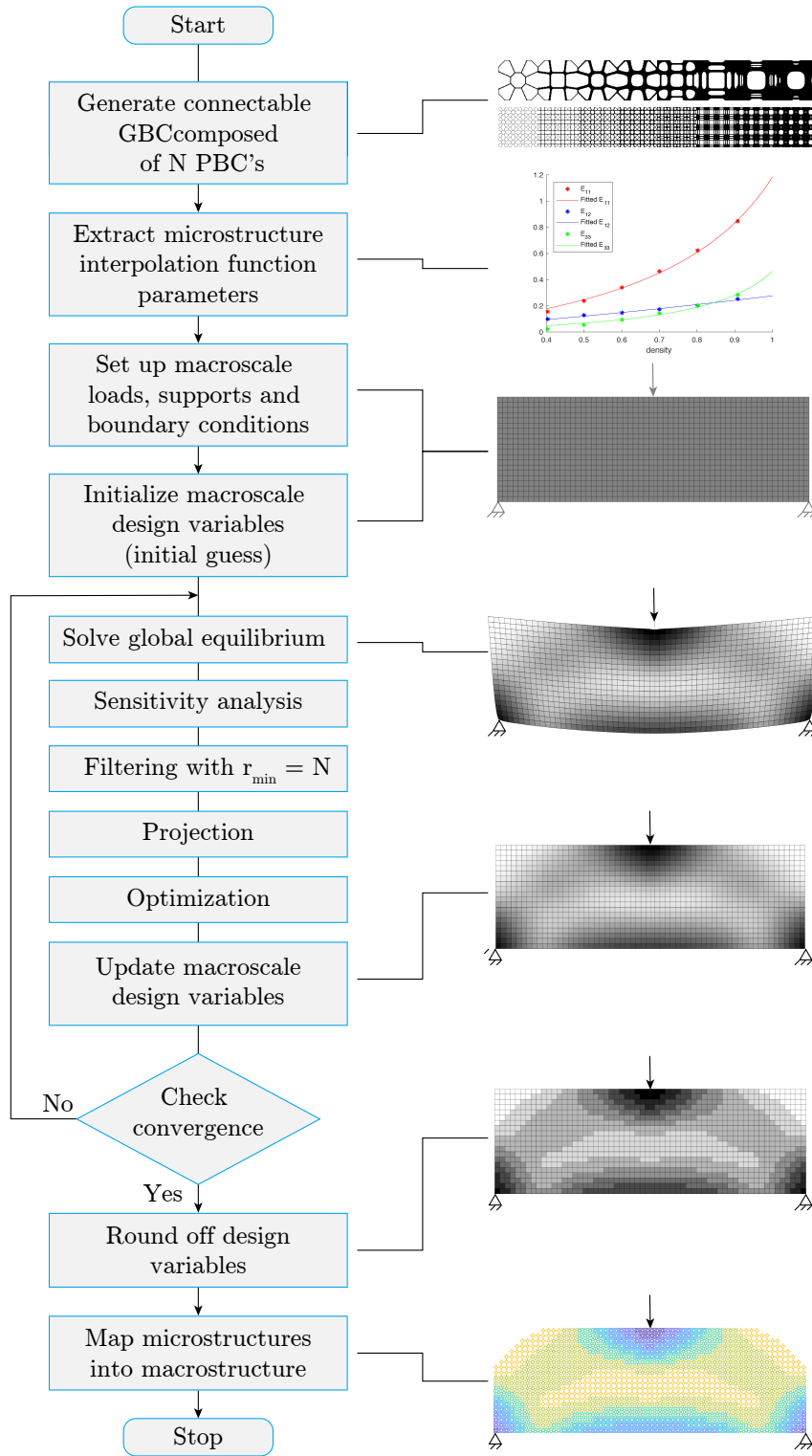
Figure 4.4: Bottom-up decoupled multiscale optimization procedure.

# 4.2 Concurrent multiscale optimization

Concurrent multiscale optimization simultaneously considers the material distribution at both the macroscopic and microscopic scales. For the minimum compliance problem, this requires simultaneous minimization of the global scale compliance and maximization of the local scale strain energy. From Rodrigues et al. (2002), the problem can be formulated as:

$$
\max_{\substack{C_{ijpq}(\mathbf{x}) \in E_{ad}\{\rho(\mathbf{x})\} \\ 0 \leq \rho(\mathbf{x}) \leq 1 \\ \int_\Omega \rho(\mathbf{x})d\Omega \leq \bar{V}}} \min_{\substack{\mathbf{u}^k \in U \\ k=1,\dots,M}} \sum_{k=1}^{M} \left( \frac{1}{2} \int_\Omega C_{ijpq}(\mathbf{x})\varepsilon_{ij}(\mathbf{u}^k)\varepsilon_{pq}(\mathbf{u}^k)d\Omega \right.
$$
$$
\left. - \int_\Omega \mathbf{p}^k \cdot \mathbf{u}^k d\Omega - \int_{\Gamma_T^k} \mathbf{t}^k \cdot \mathbf{u}^k ds \right)
\tag{4.3}
$$

The problem can be solved hierarchically by reformulating Eq.4.3 such that the point-wise minimization of strain energy is treated as a subproblem:

$$
\max_{\substack{C_{ijpq}(\mathbf{x}) \in E_{ad}\{\rho(\mathbf{x})\} \\ 0 \leq \rho(\mathbf{x}) \leq 1 \\ \int_\Omega \rho(\mathbf{x})d\Omega \leq \bar{V}}} \min_{\substack{\mathbf{u}^k \in U \\ k=1,\dots,M}} \left[ \frac{1}{2} \cdot \int_\Omega \Phi(\rho, \mathbf{u}^1, \dots, \mathbf{u}^M)d\Omega - \right.
$$
$$
\left. \sum_{k=1}^{M} \left( \int_\Omega \mathbf{p}^k \cdot \mathbf{u}^k d\Omega + \int_{\Gamma_T^k} \mathbf{t}^k \cdot \mathbf{u}^k ds \right) \right]
\tag{4.4}
$$
$$
\Phi(\rho, \mathbf{u}^1, \dots, \mathbf{u}^M) = \max_{C_{ijpq} \in E_{ad}\{\rho\}} \sum_{k=1}^{M} C_{ijpq}\varepsilon_{ij}(\mathbf{u}^k)\varepsilon_{pq}(\mathbf{u}^k)
\tag{4.5}
$$

The outer problem Eq.4.4 determines the macroscale material distribution, while the inner problem Eq.4.5 determines the homogenized material properties within each macroscale element. The optimization procedure is presented in Fig.4.5. The simply supported beam shown in Fig.4.1 is the result of a concurrent multiscale optimization procedure.
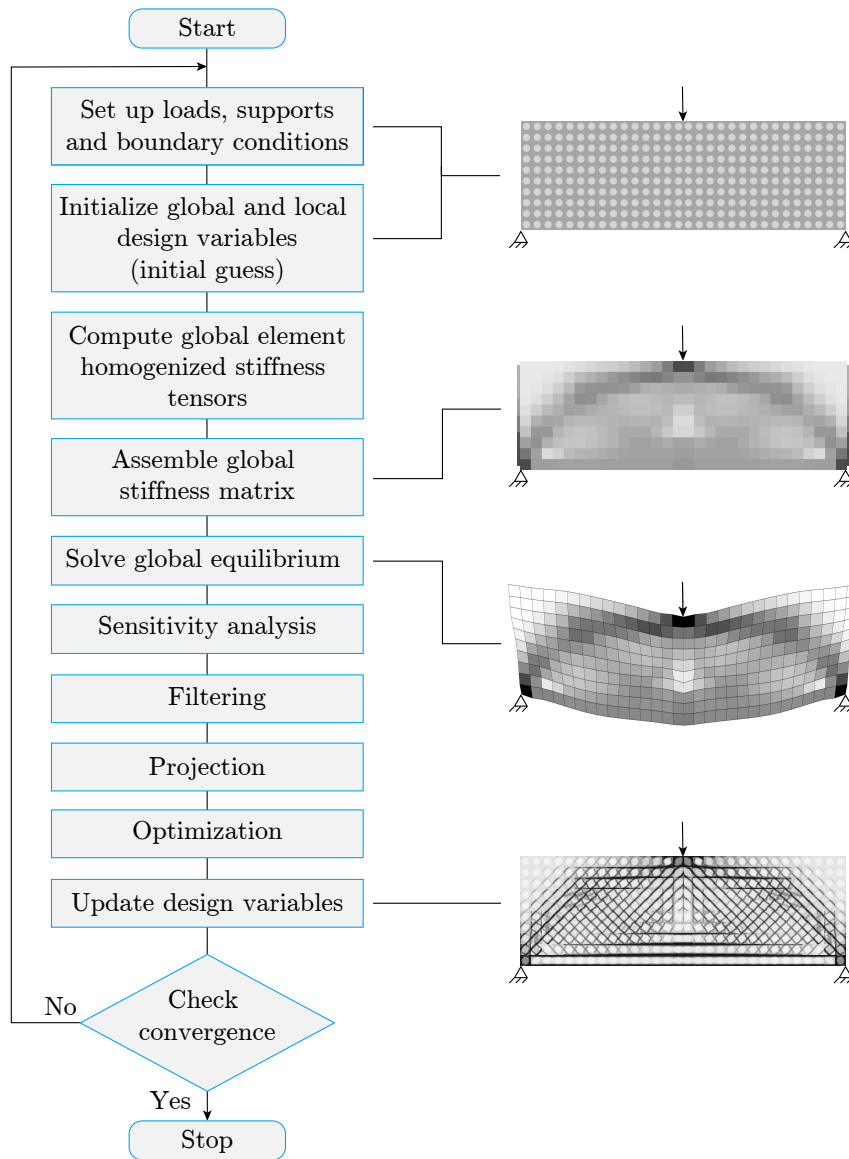
Figure 4.5: Hierarchical multiscale optimization procedure

# 5 | Connectivity issue

Functionally graded materials and multiscale structures generated using homogenization theory typically suffer from poor connectivity between adjacent microstructures, resulting in designs with unpredictable behaviour and suboptimal performance. The connectivity issue arrises because each individual periodic base cell is designed in isolation, without consideration for boundary conditions; this is an unfortunate disadvantage of homogenization theory. In the last decade, a number of approaches have been proposed to address this issue. The following section outlines these methods, highlighting their respective strengths and weaknesses.
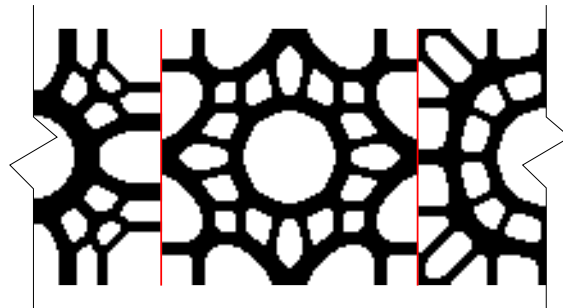


Figure 5.1: Material discontinuity between adjacent microstructures in FGM.

## 5.1 State of the art

One of the first attempts to address the connectivity issue was performed by Zhou and Li (2008). They proposed the concept of a global base cell (GBC) comprised of multiple PBC's, and systematically investigated three methods to ensure connectivity within the GBC, namely *connectivity constraint*, *pseudo-load* and *unified formulation with non-linear diffusion*.

### 5.1.1 Connectivity constraint

The connectivity constraint promotes material continuity between adjacent PBC's by forcing areas at the boundaries to be permanently occupied by solid material, as shown in Fig.5.2. Although this method generally succeeds in ensuring connectivity, it suffers from several drawbacks:

- The location of the prescribed connections must be carefully chosen, and may cause convergence to a suboptimal design.

- The algorithm may sacrifice material at the prescribed connections to achieve a better PBC design, thus failing to generate connections.

- The algorithm does not consider the overall behaviour of the GBC, which may result in unpredictable mechanical properties across the boundaries between unique PBC's.
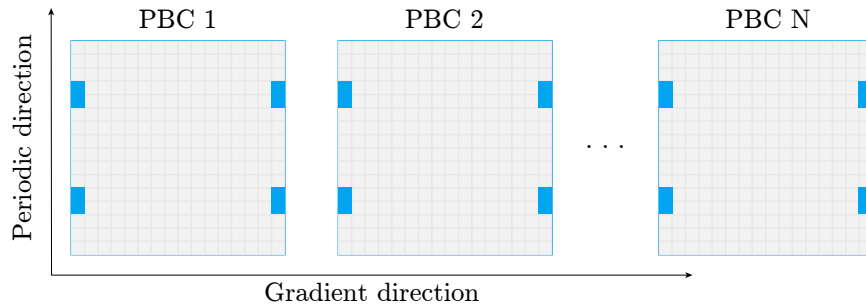


Figure 5.2: Illustration of connectivity constraint between adjacent PBC's within GBC; imposed solid regions are shown in blue. *Reproduced from Zhou and Li (2008).*

### 5.1.2 Pseudo-load

Connectivity between adjacent cells enables the FGM to withstand a tensile load. If a pseudo-load is applied to the GBC, then the application of a minimum stiffness constraint should ensure at least some connectivity between adjacent PBC within the GBC. This method was the first to directly consider the mechanical response of the FGM during the optimization procedure. However, it also suffers from several drawbacks:

- The pseudo-load conditions and minimum pseudo-stiffness are not easily defined.

- The mechanical behaviour across unit cells is not directly related to the optimization objective or to the properties of the adjacent PBC's.

- The method is not easily applicable to multi-dimensional or multiscale topology optimization problems.
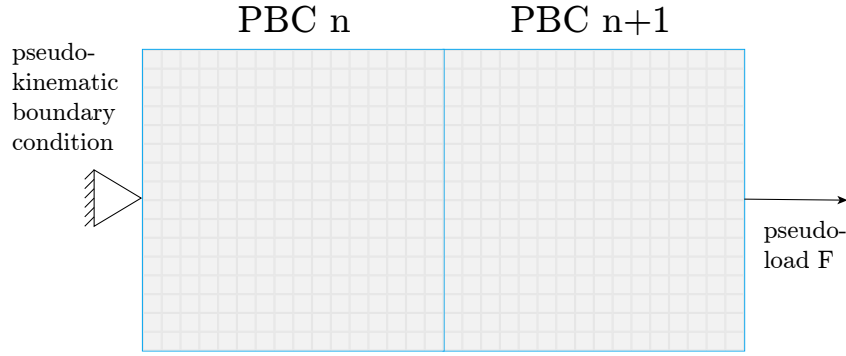
Figure 5.3: Illustration of pseudo-load method. *Reproduced from Zhou and Li (2008).*

### 5.1.3 Diffusion

The so-called *unified formulation with non-linear diffusion* considers the GBC as a whole and uses a similar filter to the one described in Section 2.3.2 to promote material deposition across PBC's. It does not guarantee connectivity, but can be used in combination with other methods to promote smooth transitions across PBC's. This application will be discussed in Chapter 5.

### 5.1.4 Structural families

Another method to ensure microstructural connectivity is to begin with a family of microstructures with parametrized topologies. The optimization objective is then to find the optimal parameter values over the design domain. An example of such a structural family is shown in Fig.5.4, from Wang et al. (2018). The downside of this method is that it fundamentally limits the design space, which inevitably leads to suboptimal solutions in most cases.
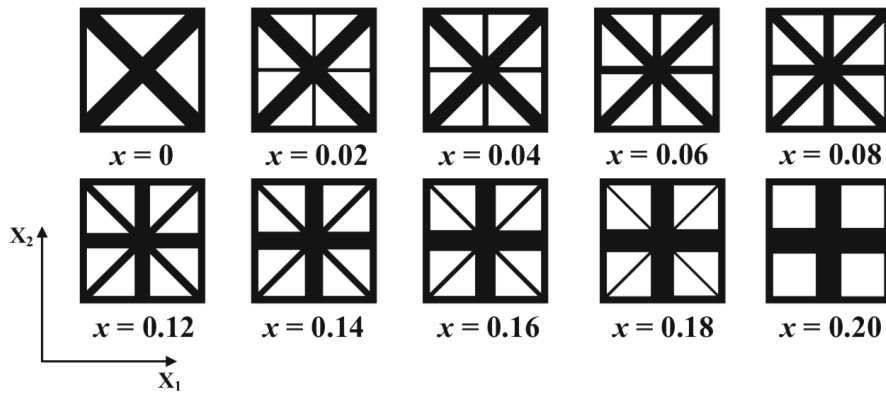


Figure 5.4: Parametrized lattice microstructures. From Wang et al. (2018).

### 5.1.5  Shape morphing

Recently, a number of geometric shape morphing techniques have been applied to the connectivity issue. Cramer et al. (2016) developed a microstructure-based material interpolation scheme in which key microstructures are first generated individually, and shape interpolation methods are used to generate intermediate structures between adjacent key structures.  Subsequently, Du and Kim (2018) used shape morphing to modify microstructural topologies post-optimization so as to maximize connectivity, while minimizing the effect on the effective mechanical properties. An example is shown in Fig.5.5, from Du and Kim (2018). Several issues arise from the application of these methods:

- The shape-interpolation technique only succeeds when the material property gradient is sufficiently small, i.e., neighbouring cells must belong to the same interpolation family (between the same key microstructures).

- The post-optimization morphing technique is sequential and the results are dependent on the order in which cells are modified.

- These methods do not consider the mechanical behaviour across adjoining cells.
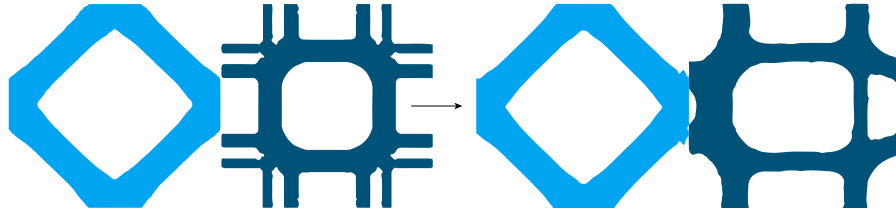


Figure 5.5:  Pre-enhancement (left) and post-enhancement (right) neighbouring microstructures, from Du and Kim Du and Kim (2018).

### 5.1.6  Progressive optimization

Radman et al. (2013) proposed a progressive optimization scheme for FGM design in which each successive PBC is designed while a filter is applied to a GBC composed of the current cell $i$, and the two previously designed cells $(i-1)$ and $(i-2)$. This method appears to be an extension of the *diffusion method* described in Section 5.1.3, with some improvement in convergence speed.

### 5.1.7 Full resolution

The most self-evident solution to the connectivity issue is to consider the full microscopic detail in the optimization procedure. This approach is extremely computationally expensive, even for 2D optimization problems. Special techniques based on contrast-independent spectral preconditioners such as the multiscale finite element method (MsFEM) have been developed to alleviate the computational burden (Lazarov, 2014). None-the-less, these methods are not yet capable of solving large scale 3D optimization problems without significant problem simplifications (Alexandersen and Lazarov, 2015).

## 5.2 Summary

Although several approaches have been proposed to address the connectivity issue, none are easily generalizable and most do not consider the mechanical behaviour of the heterogenous structure. As a result, even if adjacent microstructures possess adequate material connectivity, the performance of the structure is unpredictable. It is therefore worthwhile to develop a method which directly considers the mechanical properties across adjacent microstructures in the optimization procedure. Part II of this report presents a new approach to do just that.

# Part II

# Compound microstructural design formulation

# 6 | FGM design

In this chapter, we present a new approach to address the connectivity issue. It is applicable to FGM design, multi-physics problems and multiscale structural optimization. Instead of designing PBC's individually, we consider the mechanical behaviour of compound base cells (CBC) comprised of neighbouring PBC's. In the following section, we demonstrate the process as it applies to the design of 2D FGM with gradation in a single direction and periodicity in the other.
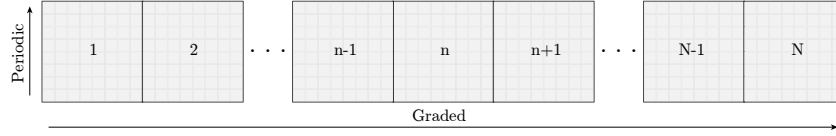


Figure 6.1: Global base cell comprised of $N$ periodic base cells.

## 6.1 Compound cell formulation

For the GBC comprised for $N$ PBC's shown in Fig.6.1, cell $n$ is considered both individually and as part of two compound base cells $[(n-1), n]$ and $[n, (n+1)]$ (see Fig.6.2 a). The optimization objective is formulated as a weighted average of the individual and compound cell properties.

$$
\begin{aligned}
\min_{\rho} \quad & \left( (1 - w_c) \sum_{n=1}^{N} c(\bar{C}_{ij}^n(\boldsymbol{\rho})) + w_c \sum_{n=1}^{N-1} c(\bar{C}_{ij}^{n,n+1}(\boldsymbol{\rho})) \right) \\
\text{s.t.} \quad & : \mathbf{K}_n \mathbf{U}_n^{A(kl)} = \mathbf{F}_n^{(kl)}, \ k, l = 1, ..., d, \ n = 1, ..., N \\
& : \mathbf{K}_{n,n+1} \mathbf{U}_{n,n+1}^{A(kl)} = \mathbf{F}_{n,n+1}^{(kl)}, \ k, l = 1, ..., d, \ n = 1, ..., N-1 \qquad (6.1) \\
& : \sum_{e=1}^{M} v_e \rho_e / |Y_n| \leq V_n \ n = 1, ..., N \\
& : 0 \leq \rho_e \leq 1, e = 1, ..., N \times M
\end{aligned}
$$

where $M$ is the number of finite elements, and for each unit cell $n$, $\mathbf{K}_n$ is the global stiffness matrix, $\mathbf{U}_n^{A(kl)}$ and $\mathbf{F}_n^{(kl)}$ are the global displacement vector and external force vector of the test case $(kl)$, respectively. Similarly, for each compound unit cell $[n, n+1]$, $\mathbf{K}_{n,n+1}$ is the global stiffness matrix, $\mathbf{U}_{n,n+1}^{A(kl)}$ and $\mathbf{F}_{n,n+1}^{(kl)}$ are the global displacement vector and external force vector of the test case $(kl)$, respectively. A weighting factor $w_c$ determines the influence of neighbouring cells on the optimization of each individual unit cell. With $w_c = 0$, this formulation is equivalent to the individual microstructure design formulation.

a)

b)

| (n-1, m+1) | (n, m+1) | (n+1, m+1) |

| n-1 | n | n+1 |

| (n-1, m) | (n, m) | (n+1, m) |

| (n-1, m-1) | (n, m-1) | (n+1, m-1) |
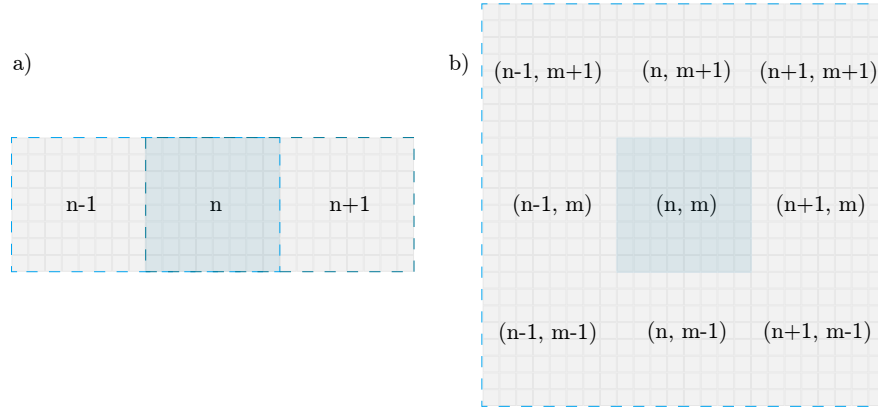
Figure 6.2: a) Cell $n$ shown as part of compound base cells $[(n-1), n]$ and $[n, (n+1)]$; b) Cell $(n, m)$ shown as part of $3 \times 3$ *superelement*.

## 6.2 FGM with 1D gradation

The FGM optimized for maximum bulk modulus shown in Fig.3.8 can be made connectable using the compound formulation with $w_c > 0$. Fig.6.3 shows the result for $w_c = 0.5$. A remarkable improvement in connectivity is achieved, at little expense to the performance of individual PBC's. The optimized properties of PBC's within the FGM are shown in Fig.6.4.



Figure 6.3: 2D FGM optimized for maximum bulk modulus with 1D linearly varying volume constraint from 20% to 90% and $w_c = 0.5$.
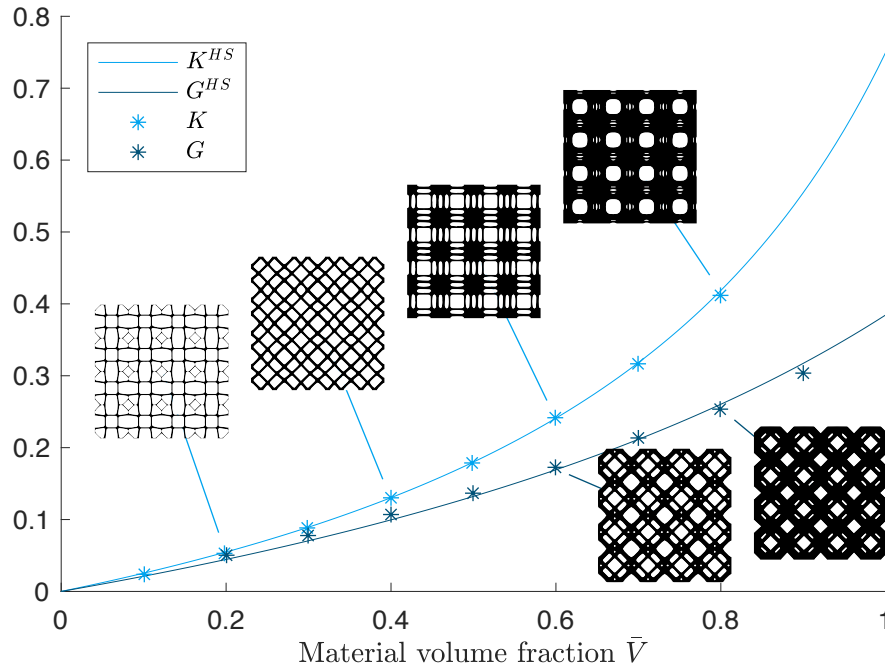
Figure 6.4:  Maximized bulk and shear moduli as a function of average material density, along with corresponding Hashin-Shtrickman theoretical bounds.

## 6.3  FGM with 2D gradation

The method can be extended to the design of FGM's with gradation along multiple directions.  The addition of a cubic symmetry constraint enables cells $i$ and $i + 1$ to be connectable along other principle axes, as can be seen in Fig.6.6.  For most optimization objectives, the symmetry constraint has little effect on the performance of individual microstructures.



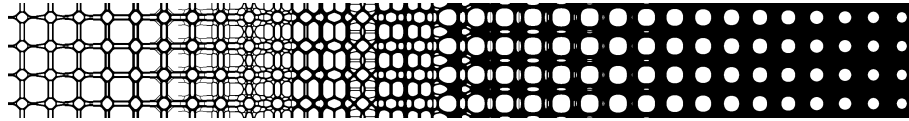Figure 6.5: 2D FGM with unit cell symmetry, optimized for maximum bulk modulus with 1D linearly varying volume constraint from 20% to 90% and $w_c = 0.5$.

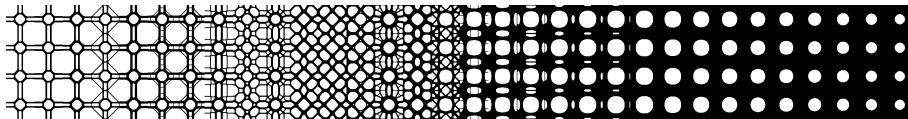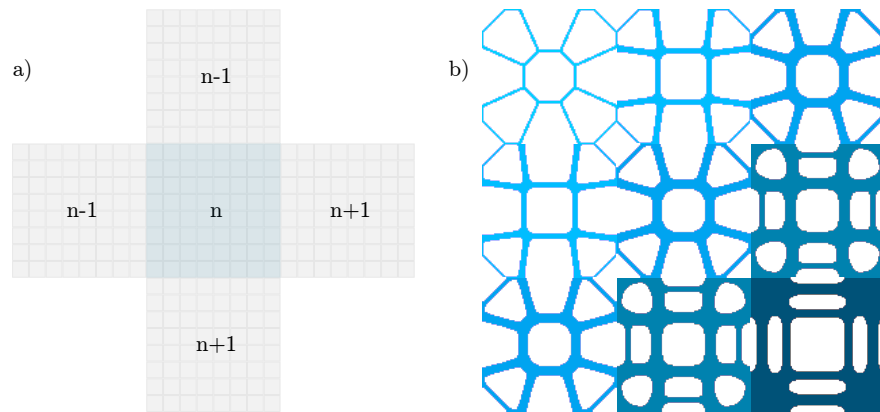Figure 6.6: a) Demonstration of bidirectional connectivity of PBC's $i-1$,$i$ and $i+1$. b) Microstructures designed with cubic symmetry constraint.
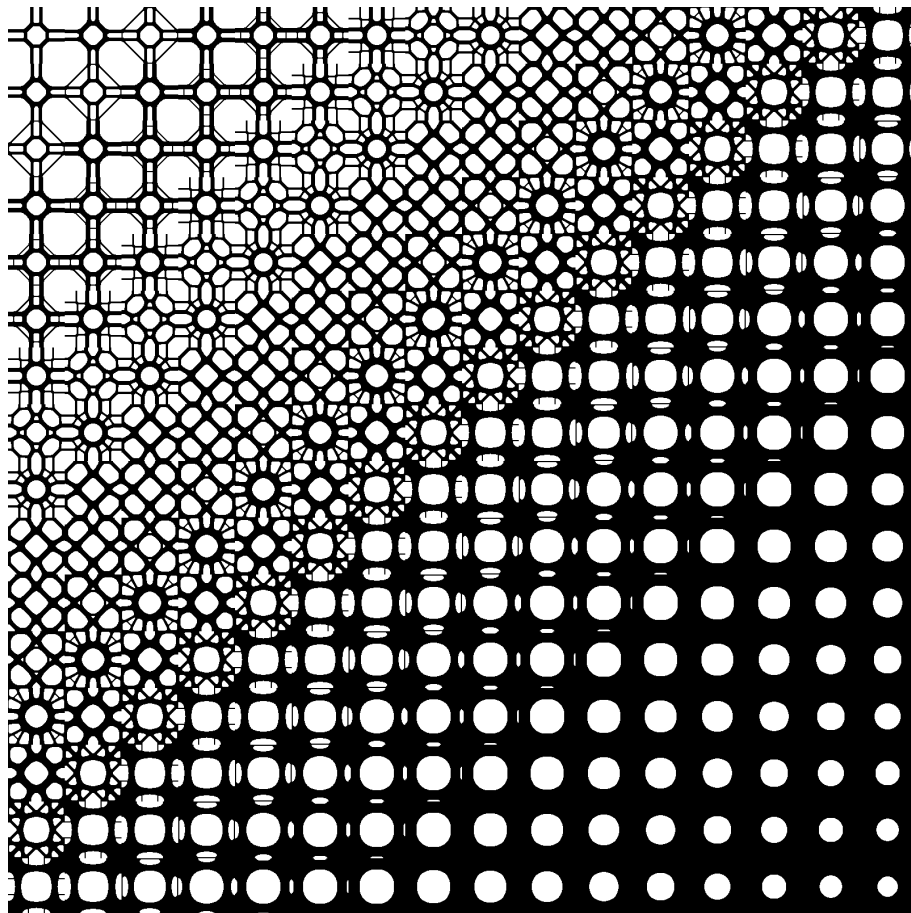


Figure 6.7: 2D FGM with symmetrical bidirectional gradation.

# 7 | Multiscale structural design

Multiscale optimization enables simultaneous material and structural design, which opens up incredible new opportunities. However, as was the case for FGM design, the typical multiscale formulation suffers from material connectivity issues. In this case, the impact is even more serious since we are interested in the performance of the global structure as opposed to the local properties within a prescribed distribution. It is therefore even more important to take into account the *physical* behaviour of adjacent microstructures.

## 7.1 Bottom-up multiscale design

The compound formulation can be applied to the bottom-up multiscale topology optimization method presented in chapter 4.1. Instead of generating the microstructures individually, we apply the compound formulation, which ensures connectivity between adjacent microstructures. Fig.7.1 shows a sound multiscale structure generated using the bottom-up approach with compound formulation.
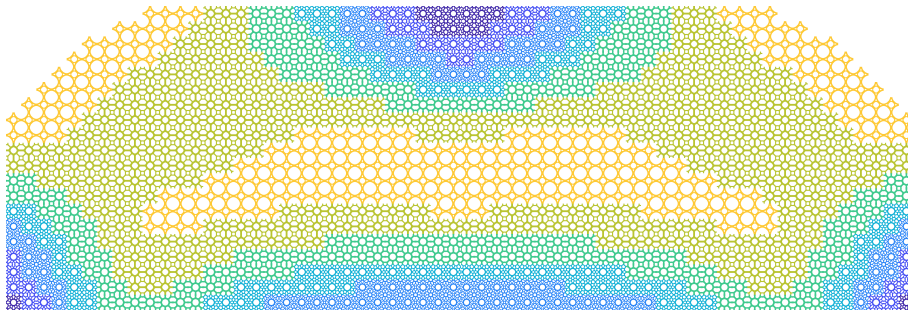


Figure 7.1: Multiscale structure generated using bottom-up approach with compound formulation.

An issue which arrises from the direct application of the compound formulation is that it requires that only small gradients be present in the macroscale material distribution, otherwise connectivity is not guaranteed. This is because the optimization scheme only considers adjacent pairs of microstructures. The formulation can be modified to ensure that all microstructures within the family are design to be compatible with one another.

$$\min_{\rho} \left( (1 - w_c^{n,m}) \sum_{n=1}^{N} c(\bar{C}_{ij}^n(\boldsymbol{\rho})) + \sum_{n,m=1,\ m\neq n}^{N} w_c^{n,m} \, c(\bar{C}_{ij}^{n,m}(\boldsymbol{\rho})) \right)$$

$$\text{s.t.} \quad : \mathbf{K}_n \mathbf{U}_n^{A(kl)} = \mathbf{F}_n^{(kl)}, \ k,l = 1,...,d, \ n = 1,...,N$$

$$: \mathbf{K}_{n,m} \mathbf{U}_{n,m}^{A(kl)} = \mathbf{F}_{n,m}^{(kl)}, \ k,l = 1,...,d, \ n = 1,...,N, \ n \neq m \qquad (7.1)$$

$$: \sum_{e=1}^{M} v_e \rho_e / |Y_n| \leq V_n \ n = 1,...,N$$

$$: 0 \leq \rho_e \leq 1, e = 1,...,N \times M$$

This formulation ensures compatibility between all microstructures, but also increases the computation cost from $O(n)$ to $O(n^2)$. It may also have an impact on the optimized performance, since it restricts the design space significantly. Fig.7.2 shows how non-adjacent pairs are compatible with one another.
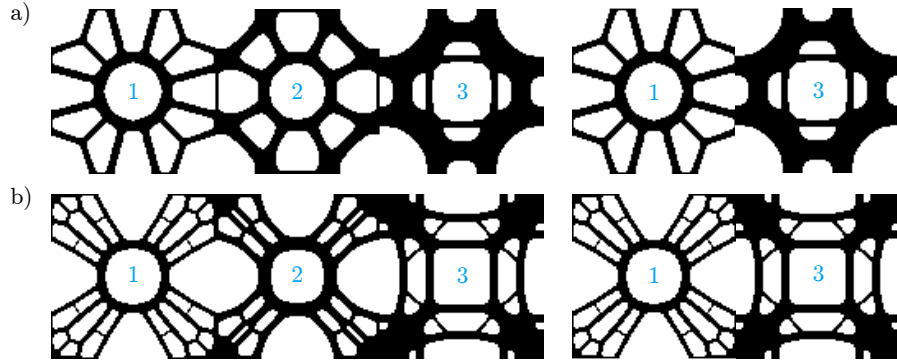


Figure 7.2: Non-adjacent pair of microstructures generated using a) original compound cell formulation, b) modified compound cell formulation.

## 7.2  Concurrent multiscale design

Concurrent multiscale optimization also suffers from the connectivity issue because the boundary conditions between adjacent microstructures are not considered in the assembly of the global stiffness matrix. In general, the ideal mechanical properties vary smoothly from cell to cell within the macro structure, but these properties can be achieved by any number of equivalent topologies. As an example, Fig.7.3 shows two cell which, individually, have identical elasticity matrices. When considered as a neighbouring pair, however, their performance is significantly diminished due to their poor material connectivity. In practice, as long as an appropriate initial design has been chosen and global filtering is employed, the connectivity issue is not widespread. However, the compound formulation can be employed to guarantee adequate compatibility.
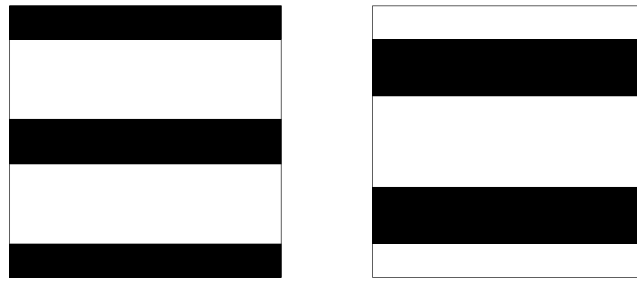
Figure 7.3: Incompatible microstructural topologies with identical mechanical properties.

We use an *in-situ* compound formulation in which the homogenized properties of each macroscale element are defined as a weighted average of the individual element stiffness tensor and a *superelement* stiffness tensor. The superelement is defined as the $3 \times 3$ (in 2D) or $3 \times 3 \times 3$ (in 3D) Moore neighbourhood centred about the element (see Fig.6.2 b). Applied in this way, the compound formulation acts as a sort of smoothing filter over the macroscale domain.

The mathematical formulation of the multiscale design problem is unchanged. The only difference is in how the homogenized stiffness tensor $\bar{C}_{ijkl}^{nm}$ is computed:

$$\bar{C}_{ijkl}^{nm} = (1 - w_c)\bar{C}_{ijkl}^{nm} + w_c\bar{C}_{ijkl}^{n\pm 1,m\pm 1} \tag{7.2}$$

Fig.7.4 and Fig.7.5 show MBB-beams generated with and without the compound formulation. The homogenization-based theoretical performance of the structures are nearly identical but the connectivity issue is reduced in the compound case. As a result, the actual performance of the structure is expected to be significantly improved. This will be investigated in Chapter 10.
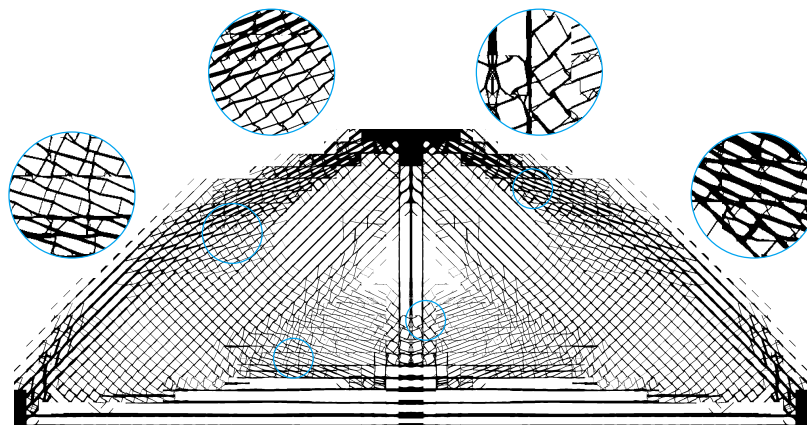


Figure 7.4: Multiscale simply supported beam under 30% volume constraint with compound formulation.
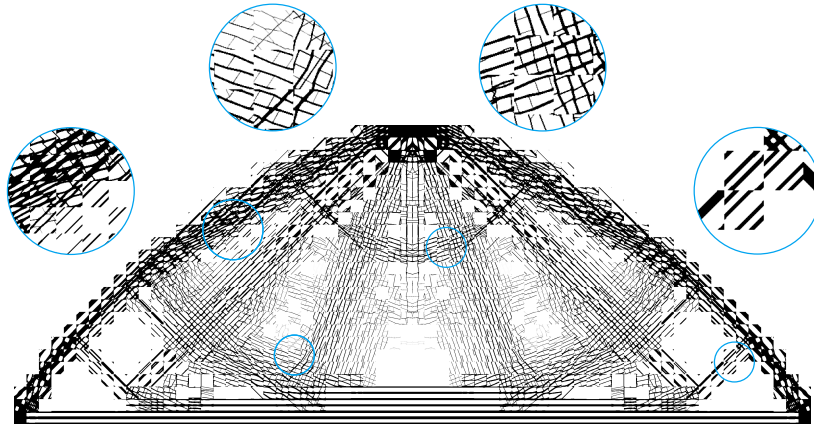
Figure 7.5: Multiscale simply supported beam under 30% volume constraint without compound formulation.

Note that the disconnected material segments at the boundaries of the structure result from the periodicity constraint and will always occur in homogenization theory-based concurrent multiscale optimization. Simple post-processing filters can be used to remove these artefacts once an optimized design has been obtained.

## 7.3 Summary

Multiscale structures generated using the compound formulation possess improved material connectivity. As a result, the actual performance of the structures is expected to be much closer to the predicted theoretical performance. In the case of concurrent multiscale optimization, the compound formulation has the added benefit of providing macroscale smoothing which prevents sharp changes in material properties from cell to cell. Since slowly changing macroscale material properties is a fundamental assumption upon which homogenization theory is based, this is expected to improve the accuracy of the repeated FEM studies within the algorithm, as well as the performance of the resulting optimized structure.

# 8 | Manufacturability considerations

Today's 3D printing technologies allow for the fabrication of structures with micro or even nano-scale features (see Fig.8.1). However, there exists an inverse correlation between printer resolution and build volume. This makes microstructural materials very challenging to fabricate at scale. To minimize this issue, we limit the required printer resolution by prescribing topological feature size restrictions on the individual unit cells. In this chapter we apply several length scale control methods to the design of microstructural materials.
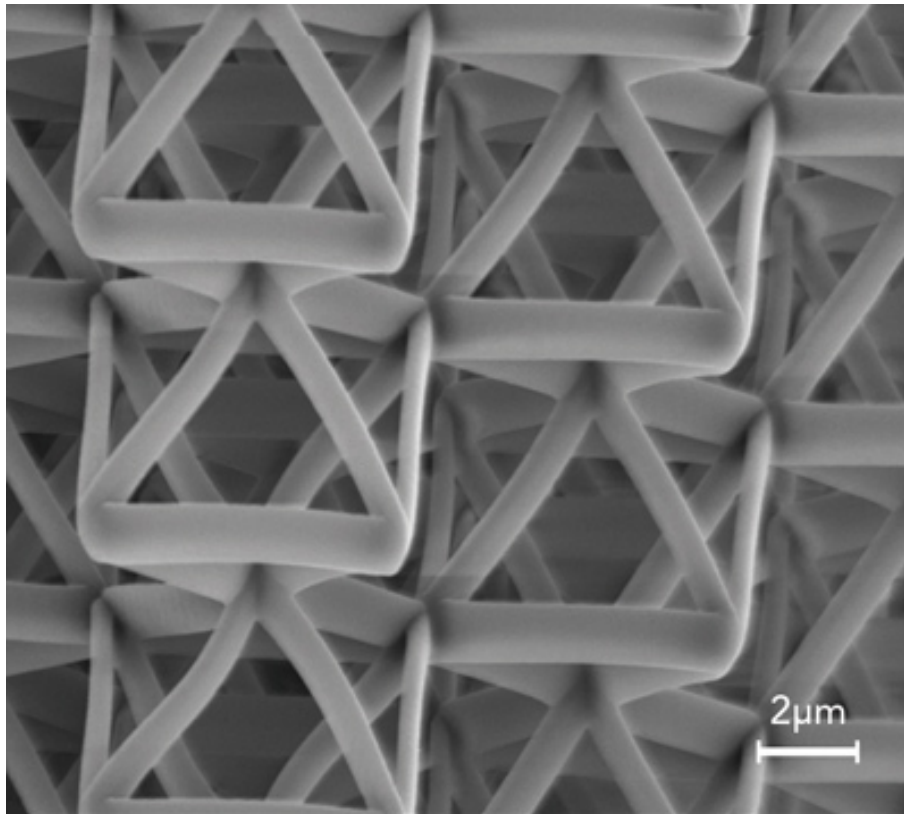


Figure 8.1: Nanoscale metamaterial fabricated with Nanoscribe 3D laser lithographic printer. *Image retrieved from Industrial laser solutions, 2015.*

# 8.1 Length scale control

By applying a minimum length scale constraint on each microstructure, we can eliminate ultra-fine detail from the optimization results. If we add an additional maximum length scale constraint, we can achieve almost uniform length scale, making it possible to use fused deposition modeling (FDM) or direct ink writing (DIW) technologies with single print paths.

## 8.1.1 Minimum length scale

To control the minimum length scale, we use the so-called *robust formulation* proposed by Wang et al. (2011). Without going into detail, this method considers additional eroded and dilated projections of the design variables to ensure that the minimum length scale is a direct function of the filter radius $r_{min}$. Fig.8.2 shows examples of microstructures optimized under different minimum length scale constraints. Interestingly, the algorithm often converges to topologies with minimum length scales greater than the imposed constraint. This can be seen in Fig.8.2 for $r_{min} = 2.1$-2.3.



Figure 8.2: Microstructures optimized for maximum bulk modulus under different minimum length scale constraints and subject to 40% volume constraint.

## 8.1.2 Maximum length scale

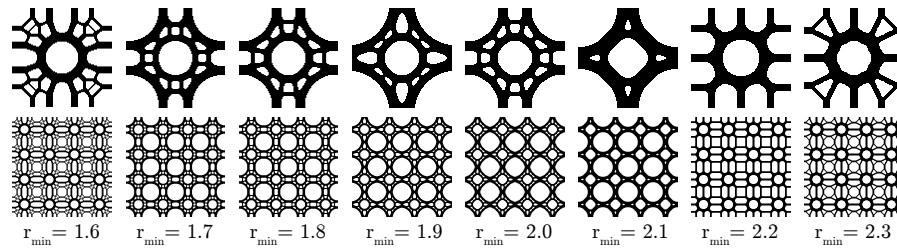To control the maximum length scale, we add a local volume constraint, as proposed by Wu et al. (2018). This constraint restricts the accumulation of material in any region of the unit cell, effectively limiting the maximum length scale and minimum pore size. In mathematical form, the constraint is written as

$$\bar{\rho}_e \leq \alpha, \forall e \tag{8.1}$$

where $\alpha$ is the prescribed local volume fraction and $\bar{\rho}_e$ is the average volume fraction in the neighbourhood $\mathbb{N}$ of $e$, i.e.,

$$\bar{\rho}_e = \frac{\sum_{i \in \mathbb{N}_e} \rho_i}{\sum_{i \in \mathbb{N}_e} 1} \tag{8.2}$$

and the neighbourhood $\mathbb{N}$ is the set of elements within a radius $R_e$ of element $e$, i.e.,

$$\mathbb{N}_e = \{i| \ ||x_i - x_e||_2 \leq R_e\} \tag{8.3}$$

where $x_e$ and $x_i$ are the centroids of the element and neighbouring elements, respectively. The maximum length scale is a function of both $R_{min}$ and $\alpha$. Fig.8.3 shows microstructures optimized with different values of $\alpha$, and Fig.8.4 shows microstructures optimized with different values of $R_{min}$.
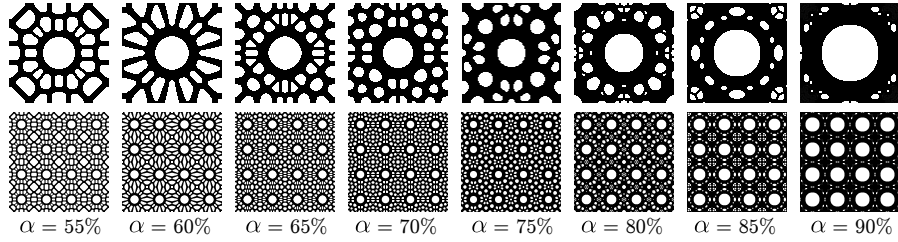


Figure 8.3: Microstructures optimized for maximum bulk modulus under local volume constraint with different values of $\alpha$ and $R_{min} = 26$.
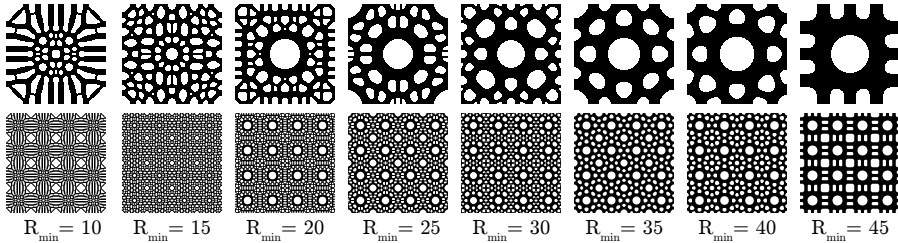


Figure 8.4: Microstructures optimized for maximum bulk modulus under local volume constraint with different values of $R_{min}$ and $\alpha = 70\%$.

## 8.2  Global filtering

It is also important to avoid sharp edges within and across adjacent microstructures. This helps eliminate stress concentrations and reduces manufacturing complexity. We apply a filter across the entire GBC, similar to the *diffusion* technique proposed by Zhou and Li (2008). Instead of a non-linear filter, we simply apply the mesh-independency filter presented in Chapter 2. In Fig.8.5, GBC's optimized with and without global filtering are compared. Note that the filter often changes the topology of the unit cells, but has little effect on the objective function.
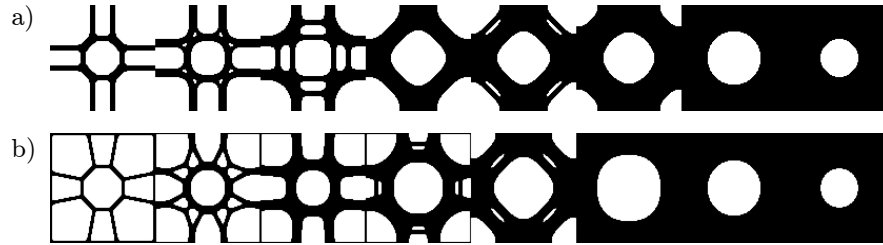


Figure 8.5: GBC optimized for maximum bulk modulus under linearly varying volume constraint from 20% to 90% a) without global filtering; b) with global filtering.

## 8.3  Summary

Even as 3D printing technologies mature, the needs for large build volumes and high resolutions will be at odds. This issue is especially important to take into consideration in the design of microstructural materials. We demonstrate the use of length scale control methods and global filtering in reducing the printer resolution requirements.

# Part III

# Results & discussion

# 9 | Design examples

In this section, we present examples of microstructures designed using our compound formulation. We focus on three applications: functionally graded orthopaedic hip implants with prescribed property distributions, non-convergent single scale optimization, and multiscale structures with prescribed boundary geometry.

## 9.1 Functionally graded prosthetic implant

Building on the work of Kolken et al. (2018), we apply our method to the design of meta-biomaterials aimed at improving the longevity of orthopaedic implants. Specifically, we aim to achieve better implant fixation by generating a structure with high porosity at the bone-implant interface. This is expected to promote dendritic bone ingrowth, which will effectively fuse the bone and implant together. Here we focus on applications in total hip replacement surgeries (see Fig.9.1), which typically suffer from low lifespans due to aseptic loosening, resulting from poor implant fixation.
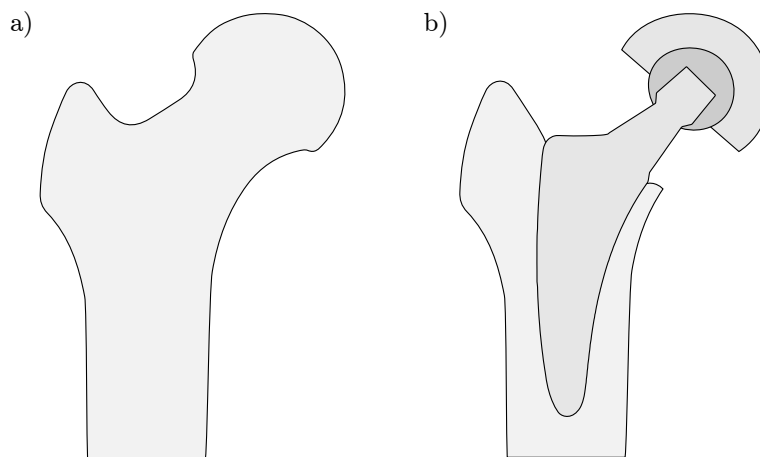


Figure 9.1: Femur before (a) and after (b) total hip replacement surgery.

We first define a macrostructural gradation with high porosity and the bone-implant interface and high density in the core region (1). We then generate a family of compatible microstructures optimized for maximum bulk modulus under linearly varying porosity constraint (2). Finally, we map the microstructures into the macroscale distribution (3). Fig.9.2 shows the process in 2D. Fig.9.4 shows a titanium specimen fabricated using a GmbH SLM125 selective laser melting machine.
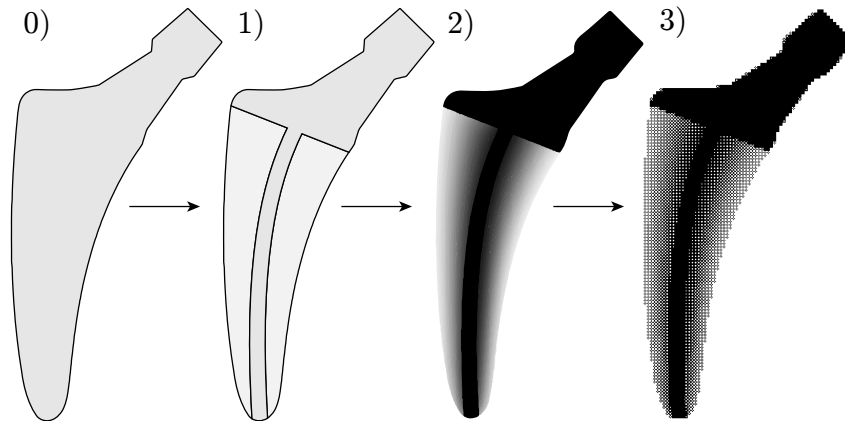


Figure 9.2: Procedure for generating bio-compatible orthopaedic hip implant.
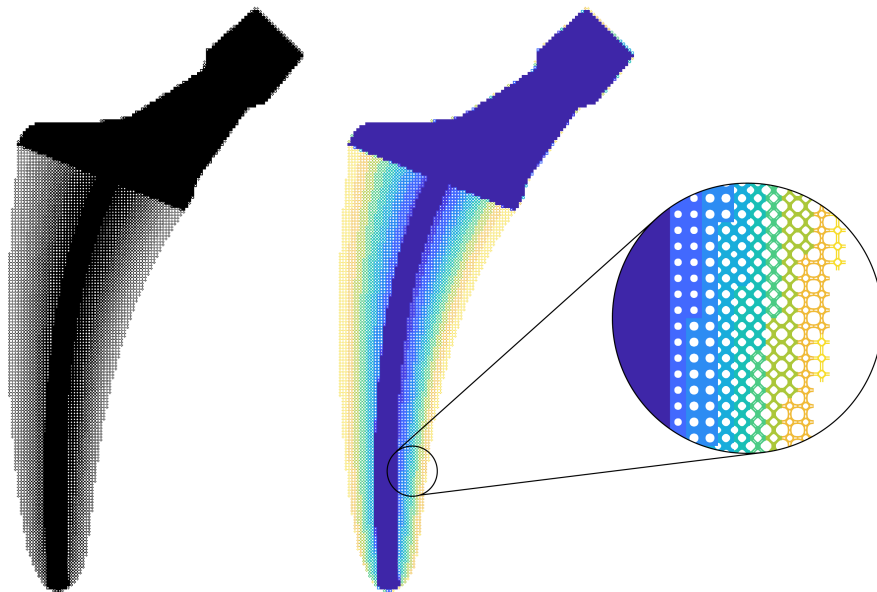


Figure 9.3: Functionally graded orthopaedic implant

Figure 9.4: .
Specimen fabricated using selective laser melting (SLM). Material: Ti-6Al-4V ELI
(Extra Low Interstitials) ASTM B348 with a particle size range of 10-45 micron,
Machine: GmbH SLM125

### 9.1.1  Bone ingrowth

It is difficult to visualize how the increased porosity promotes dendritic bone ingrowth based on the 2D renders since there are no physical connections between neighbouring pores. In 3d, however, this is usually not the case. Fig.9.5 shows a 3D microstructure optimized for maximum bulk modulus. Here, the void region is connected to its neighbours on all sides. Unfortunately, there is no guarantee that this will be the case in all optimization results. In general, the addition of some sort of *fluid permeability* constraint is necessary to ensure pore connectivity (Guest and Prévost, 2006).
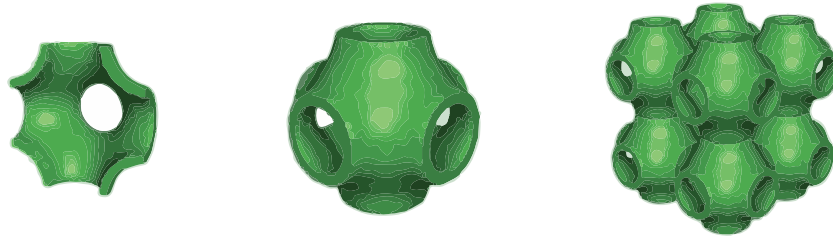


Figure 9.5: Three-dimensional microstructure with maximum bulk modulus. *Reproduced from Radman et al. (2013).*

## 9.2 Non-convergent structures

In some cases, topology optimization problems suffer from lack of convergence. In many cases, this issue can be resolved with the addition of projection methods or filtering techniques (Guest et al., 2004). However, in certain cases, the best solution is in fact non-binary. In such cases, it would be better to generate microstructures with the mechanical properties of these intermediate density elements and map them into the structure. The bottom-up optimization approach desc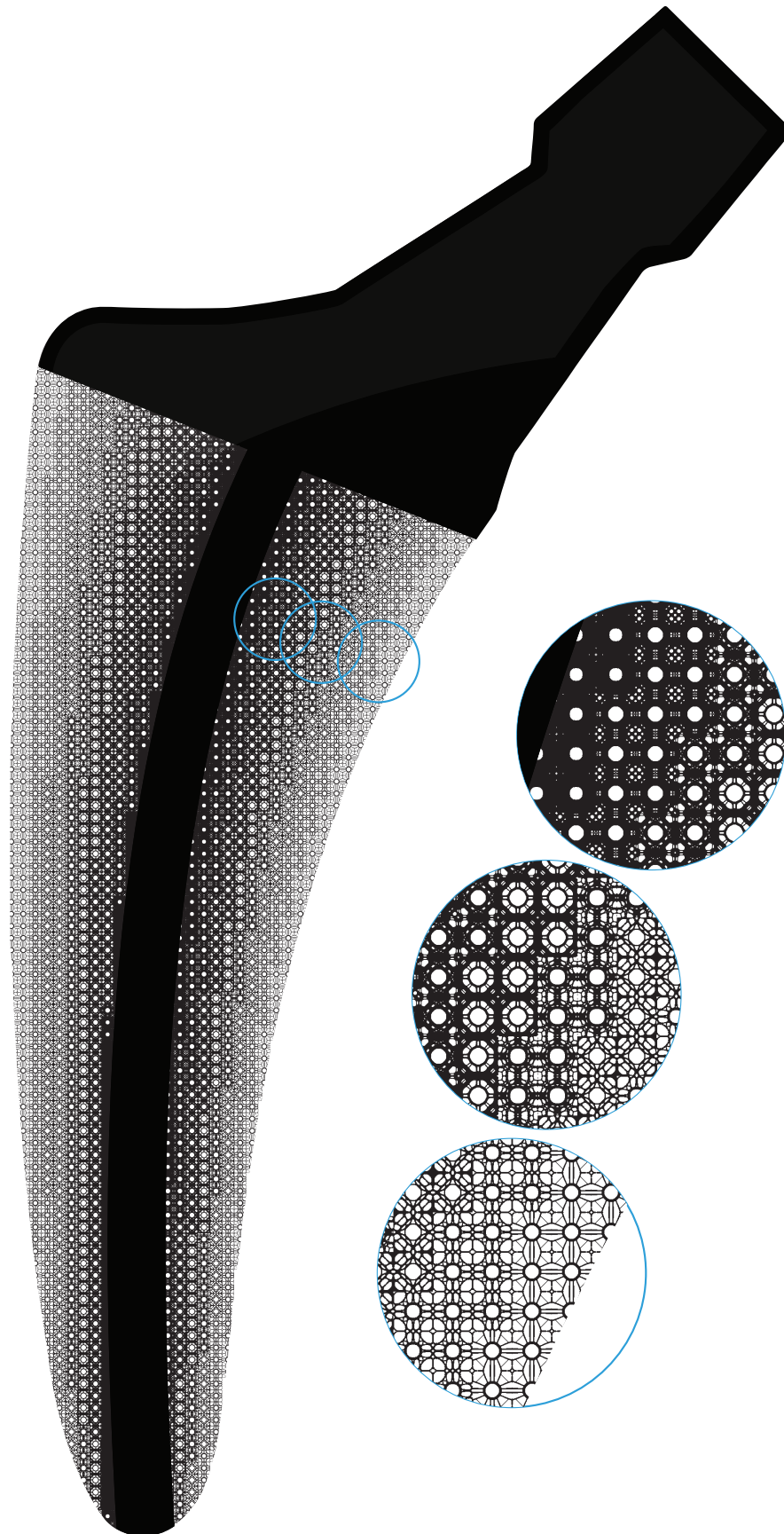ribed in Section 4.1 is well suited to this task. In Fig.9.6, the process is applied to the design of a fixed beam with a distributed load and subjected to a local material constraint. The problem is initialized in (1). A set of isotropic microstructures are generated, and their stiffness tensors are used to generate an interpolation scheme, which is in turn used to solve the macroscale optimization problem (2). The macroscale design variables are then discretized (3) and replaced with their corresponding microstructures (4). Fig.9.7 shows the final microstructural distribution, highlighting the connectivity in a high contrast region of the macrostructure. In Chapter 10, we compare the performance of the multiscale structure to the theoretical performance of the greyscale solution.
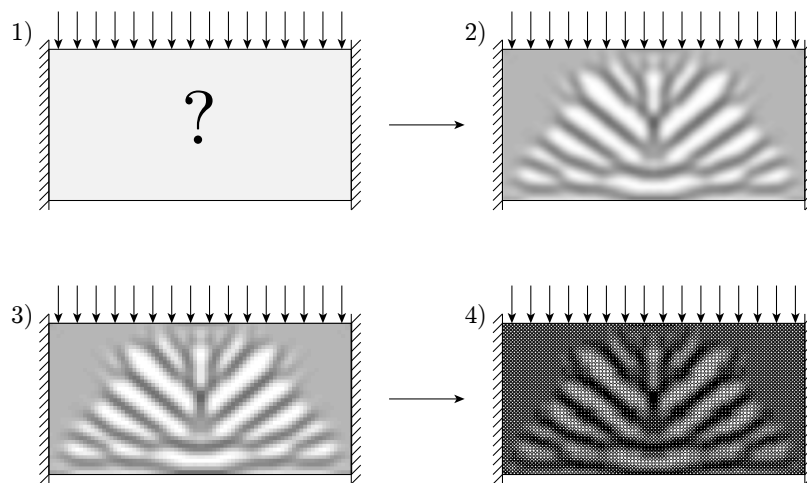


Figure 9.6: Bottom-up multiscale procedure applied to fixed beam with distributed load and local volume constraint ($\alpha = 0.6, r_{min} = 22$).
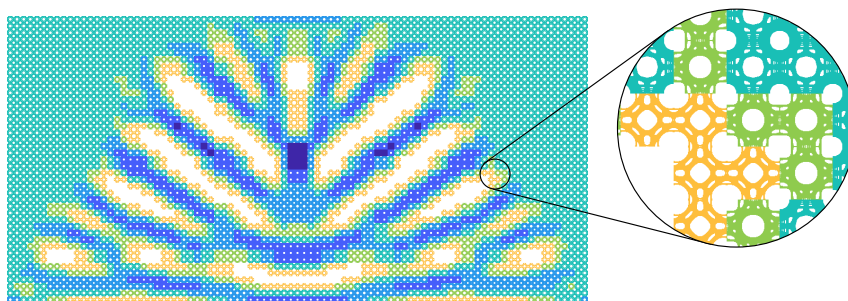


Figure 9.7: Result of bottom-up optimization applied to fixed beam with distributed load and local volume constraint ($\alpha = 0.6, r_{min} = 22$).

## 9.3 Structures with prescribed boundary geometry

The connectivity issue becomes especially apparent in concurrent multiscale optimization when a design domain is bounded by a prescribed microstructure. In the following example, a cantilevered beam with a prescribed shell structure is optimized for maximum stiffness. The compound formulation ensures that the final structure is well connected both internally and with respect to the prescribed shell geometry.

Figure 9.8: Multiscale cantilevered beam with prescribed shell microstructure optimized without the compound formulation ($w_c = 0.1$).
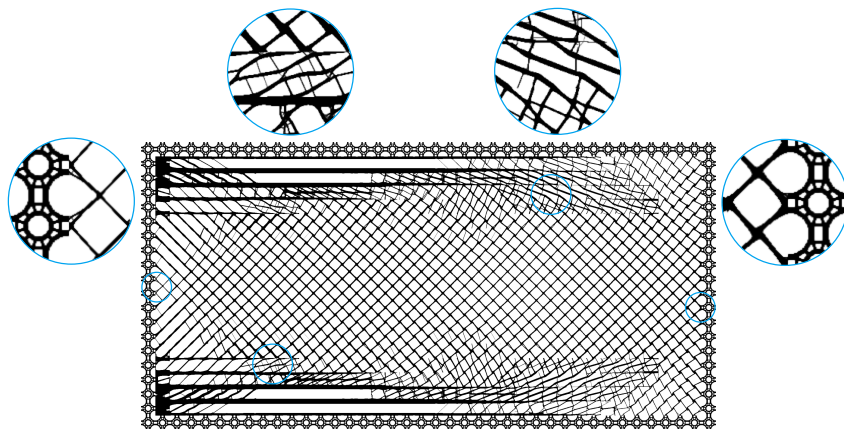


Figure 9.9: Multiscale cantilevered beam with prescribed shell microstructure optimized with the compound formulation.

# 10 | Numerical validation

In this chapter, we evaluate the effectiveness of the compound formulation in its different forms. Firstly, we evaluate microstructural connectivity by comparing the properties of compound cells to those of their constituent microstructures. Secondly, we assess the impact of the compound formulation on the properties of individual microstructures. Finally, we evaluate the performance of multiscale structures via full resolution FEM studies.

## 10.1 Connectivity and compatibility

To assess microstructural connectivity, prior works measured the fraction of connecting material across cell boundaries. This method provides some indication of connectivity, but may fail to provide an accurate representation if the algorithm chooses to sacrifice material at the cell boundaries. Moreover, it does not consider the mechanical properties across adjacent cells. As a result, the structures may behave unpredictably, even if they are well connected. Instead, we investigate the properties of compound cells comprised of adjacent microstructures. We compare these properties to those of the constituent microstructures and to those of the theoretical bounds. The results are plotted in Fig.10.1 and Fig.10.2.



Figure 10.1: Optimized properties across adjacent cells with and without compound formulation, without global filtering.
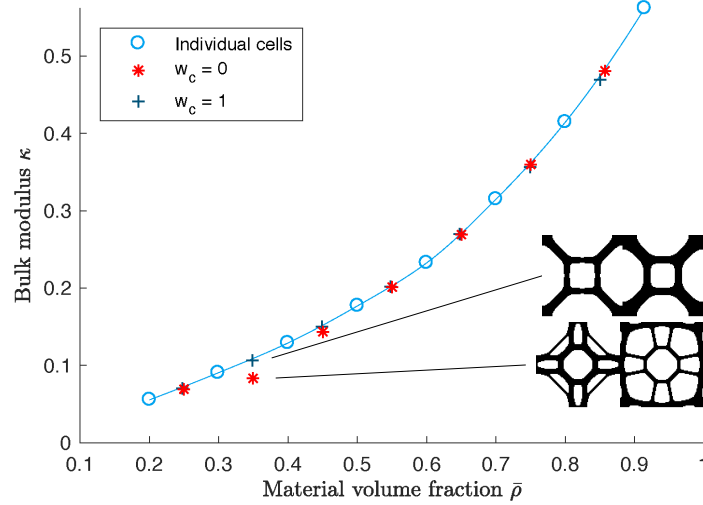
Figure 10.2: Optimized properties across adjacent cells with and without compound formulation, with global filtering.

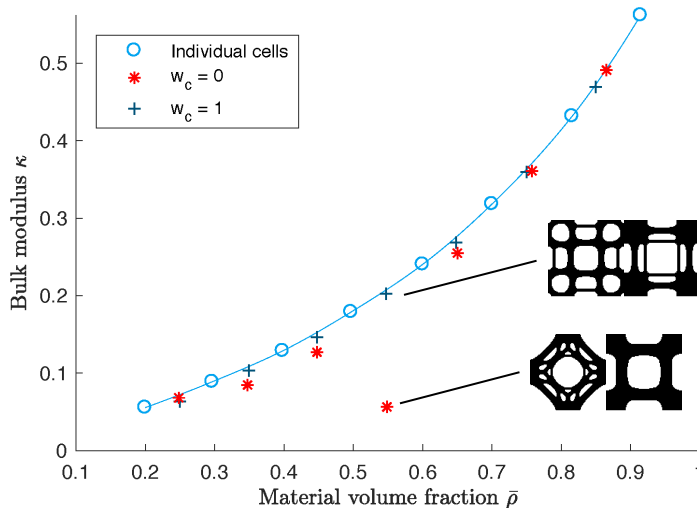The results show that without the compound formulation, mechanical properties across adjacent cells are often far from optimal. In fact, in many cases, they are inferior to those of either of the constituent cells. This is consistent with a visual connectivity assessment. With the compound formulation applied, properties across adjacent cells are very close to the theoretical bounds and always between those of the constituent cells. This appears to be the case for all values of $w_c > 0$.

## 10.2  Parameter study: Weighting factor $w_c$

The compound weighting factor $w_c$ determines the degree to which the behaviour of the compound unit cells affects the objective function. With $w_c = 0$, only the individual cells are considered and no connectivity constraint is applied. With $w_c = 1$, only the compound cells are considered in the objective function.

Families of eight microstructures (GBC) optimized for maximum bulk modulus were generated with values of $w_c$ from 0 to 1 by increment of 0.1. GBC's generated with different values of $w_c$ are shown in Fig.10.5. The impact on the optimized properties is defined as: $(c_0 - c_{w_c})/c_0$, where $c_0$ and $c_{w_c}$ are the objective function values with weighting factor equal 0 and $w_c$, respectively. Fig.10.6 shows the impact factor as a function of $w_c$. The study was performed with and without global filtering applied.
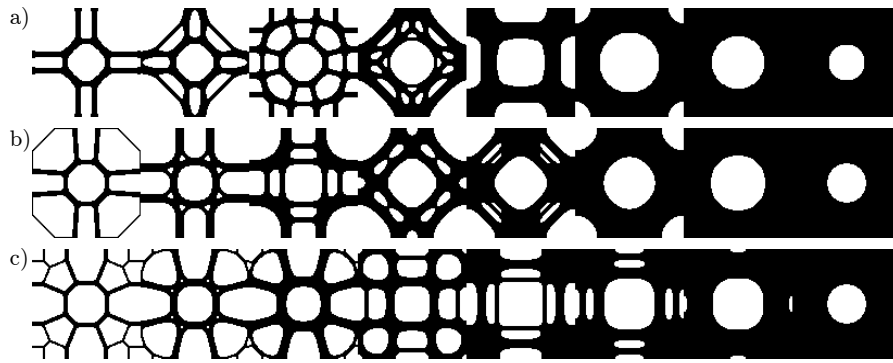
Figure 10.3: GBC's optimized for maximum bulk modulus without global filtering under linearly varying volume constraint from 20% to 90% and a) $w_c = 0.0$, b) $w_c = 0.5$, c) $w_c = 1.0$.
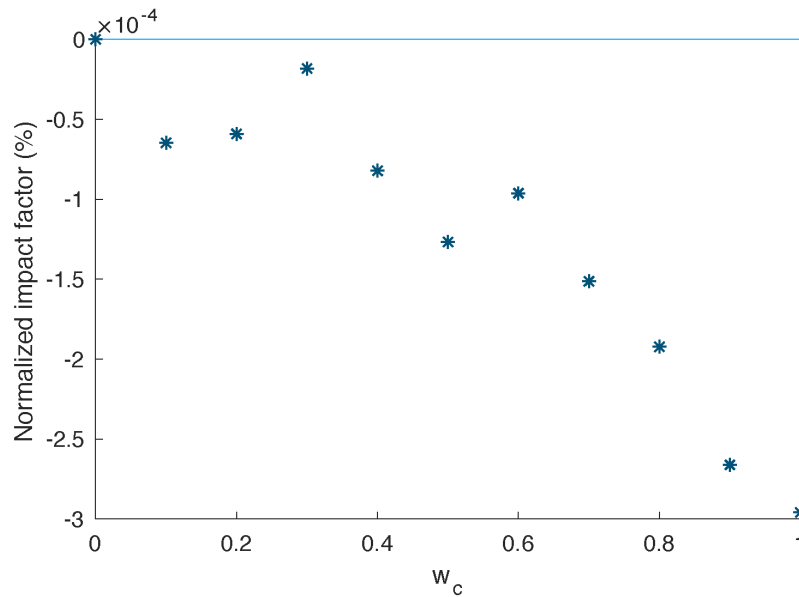


Figure 10.4: Average normalized impact on bulk modulus as a function of $w_c$, for 8 cell GBC's optimized for maximum bulk modulus without global filtering under linearly varying volume constraint from 20% to 90%.
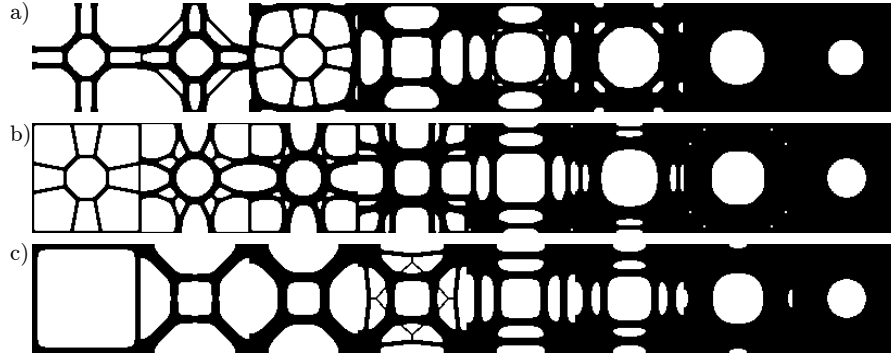
Figure 10.5: GBC's optimized for maximum bulk modulus with global filtering under linearly varying volume constraint from 20% to 90% and a) $w_c = 0.0$, b) $w_c = 0.5$, c) $w_c = 1.0$.
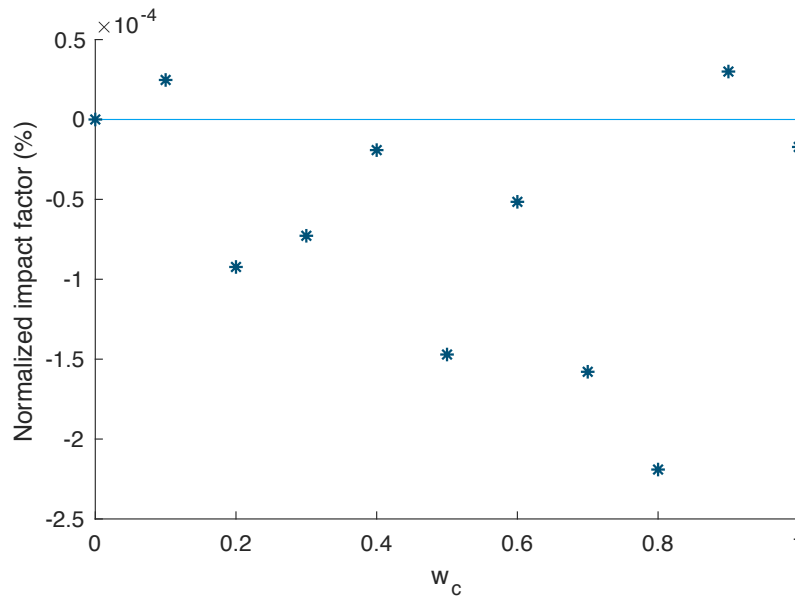


Figure 10.6: Average normalized impact on bulk modulus as a function of $w_c$, for 8 cell GBC's optimized for maximum bulk modulus with global filtering under linearly varying volume constraint from 20% to 90%.

The results show that the compound formulation has negligible impact on the optimized properties of individual microstructures ( $< 0.001\%$) . Moreover, there does not appear to be any correlation between the value of $w_c$ and the impact factor. For the design of FGM with maximized mechanical properties, it appears that $w_c = 1$ is a suitable parameter setting. This means that individual cells can be ignored in the optimization procedure, reducing the number of FEM studies from $2n - 1$ to $n - 1$ per iteration. We also note that the resulting topologies are very different from one GBC to another. This supports the conclusion from previous works that identical properties can be achieved via any number of different topologies.

## 10.3 Full resolution FEM studies

Homogenization theory states that a set of averaged mechanical properties can be obtained from the study of a single unit cell, and that an infinitely dense array of this unit cell will have nearly the same mechanical properties. In this section, we compare the homogenization-based performance of multiscale structures to full resolution FEM studies. We make use of the multigrid conjugate gradient preconditioner algorithm from Amir et al. (2014) to handle the large problem sizes.

### 10.3.1 FGM study

A macrostructure comprised of two material regions, is loaded as shown in Fig.10.7. Each region is prescribed a microstructure, designed to be compatible with its neighbour via the compound formulation. The compliance of the structure is then evaluated first using the homogenized properties of the two microstructures and then via full resolution FEM studies, with various array densities. Fig.10.8 shows the normalized results as a function of microstructural array density. The results indicate that even for relatively coarse microstructural arrays, the compliance values computed via homogenization are within 5% of the full resolution FEM results. In contrast, the compliance of a macrostructure comprised of microstructures designed without the compound formulation perform is several orders of magnitude larger than predicted by homogenization theory. The results are included in Table **??**.
The fact that homogenization theory does indeed hold for this multi-metamaterial structure confirms that the compound formulation succeeded in generate compatible microstructures.
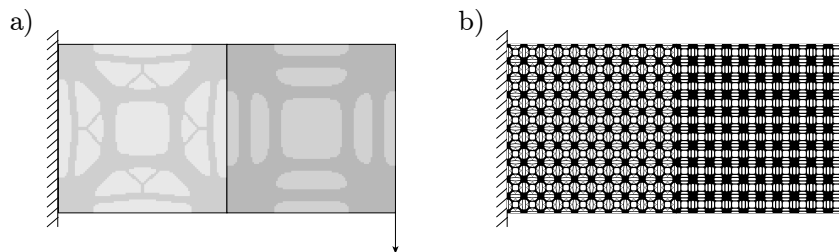


Figure 10.7: Test structure comprised of two microstructural regions. a) Homogenized material distribution; b) Finite length scale microstructural distribution with array density $m = 10$.
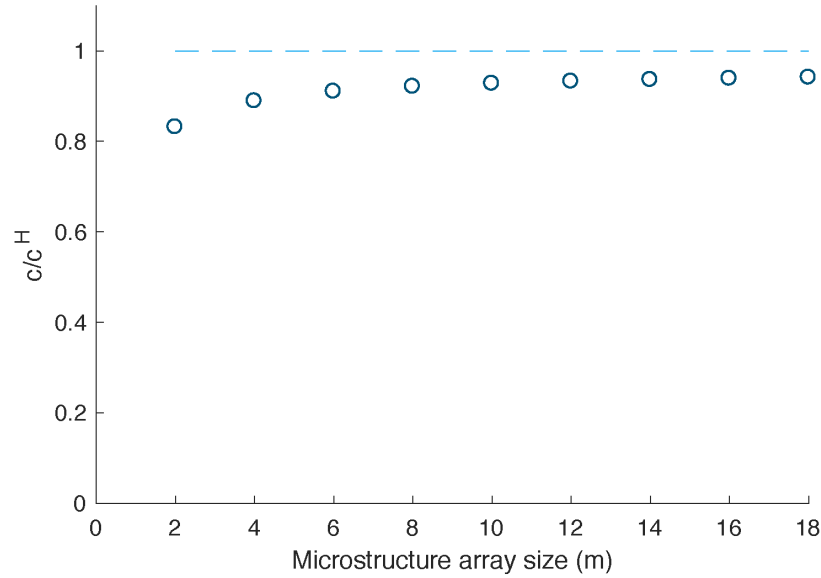
Figure 10.8: Normalized compliance vs. microstructural array density for test structure described in Fig.10.7.

### 10.3.2 Multiscale study

We apply the same methodology to the study of multiscale structures. We consider the multiscale MBB-beams shown in Fig.7.1 and Fig.7.4 optimized for minimum compliance using the bottom-up and concurrent multiscale algorithms. The compliance of the optimized structures are evaluated using full resolution FEM and compared to the results homogenization-based multiscale algorithms.

Table 10.1: Results of full resolution FEM analysis for structures generated with and without compound multiscale formulation

|  | Compliance | | | |
|  | Standard formulation | | Compound formulation | |
|  | Homogenized | Full resolution | Homogenized | Full resolution |
|---|---|---|---|---|
| FGM ($m = 10$) | $2.436 \times 10^2$ | $1.899 \times 10^8$ | $2.862 \times 10^2$ | $2.892 \times 10^2$ |
| Bottom-up MBB | $3.536 \times 10^{19}$ | $6.735 \times 10^{28}$ | $3.536 \times 10^{19}$ | $5.121 \times 10^{20}$ |
| Concurrent MBB | $6.354 \times 10^4$ | $4.842 \times 10^{10}$ | $7.453 \times 10^5$ | $1.532 \times 10^7$ |

As expected, the full resolution structures perform worse than the homogenized structures. However, the structures generated using the compound formulation perform significantly better than those generated with the state-of-the-art algorithms. This can be attributed to the improved connectivity and compatibility between adjacent microstructures.

# 11 | Conclusions and recommendations

## 11.1 Conclusions

The design and realization of functionally graded metamaterials, whose spatially-varying physical properties are a function of their microstructural geometry, is particularly challenging because the underlying mathematical model does not take into account the physical boundary conditions between adjacent microstructures. As a result, the optimized structures do not perform as expected and are often impossible to fabricate. In this work, we proposed a compound cell formulation which directly considers the mechanical properties across adjacent microstructures to ensure both geometric connectivity and mechanical compatibility. In our formulation, microstructures are generated based on the performance of both individual unit cells and compound unit cells comprised of neighbouring pairs. In contrast to existing methods, our approach is generalizable and can be applied to multiscale and multi-physics problems. It is also easily integrated into many existing topology optimization algorithms, density-based or otherwise.

We applied our method to the design of single and multidimensional functionally graded materials and to the design of multiscale structures. The results show improved connectivity at no expense to the performance of individual microstructures. This observation supports the notion that many microstructural topologies may share the same mechanical properties. The compound formulation simply promotes convergence to compatible microstructures. Furthermore, we compared the performance of full resolution structures generated with and without the compound formulation to the homogenization-based predictions and observed a significant improvement in accuracy when the compound formulation is applied.

Even with improved microstructural connectivity, the fabrication of metamaterials and multiscale structures presents significant challenges. Homogenization theory is only accurate if the microscopic length scale is very small compared to the macroscopic length scale. As a result, any 3D printing technologies employed in the fabrication of these structures must be both extremely precise and possess large build volumes. To reduce the required precision, we applied state-of-the-art length scale control methods to the design of microstructural materials. We were able to control both minimum and maximum length scales on both material and voids. Moreover, we applied global smoothing to reduce the occurrence of sharp edges, which are nearly impossible to fabricate in practice.

## 11.2  Recommendations

*Multi-physics*

Although the examples presented in this work related to the optimization of mechanical properties, the proposed method can also be applied to the development of materials with gradations in other functional properties such as electrical permittivity, thermal conductivity, magnetic permeability, vibration dampening, etc. In fact, the compound formulation can be applied to most optimization problems in which spatially-varying objectives or constraints exist.

*Three dimensions*

The examples presented in this work were all 2 dimensional in nature. The method is equally applicable in 3 dimensions. However, the computational cost of such procedures will be much larger and parallel processing techniques will need to be employed to ensure sufficiently rapid convergence.

*Experimental validation*

Due to the limitations of current 3D printing technologies, the work presented in this report cannot be experimentally validated. Although we have performed full resolution FEM studies, future work in this area would benefit from physical prototyping and testing.

*Pore size control*

In applying a local material volume constraint to control the maximum length scale, we realized that the size of voids of the material could also be controlled to some extent. The ability to prescribe pore size may be useful to promote dendritic bone ingrowth in the design of orthopaedic implants. This may be an interesting opportunity for further investigation.

# Bibliography

How topology optimization changed the design process. In C. A. Motasoares, J. A. C. Martins, H. C. Rodrigues, Jorge A. C. Ambrósio, C. A. B. Pina, C. M. Motasoares, E. B. R. Pereira, and J. Folgado, editors, *III European Conference on Computational Mechanics*, pages 495–495. Springer Netherlands, Dordrecht, 2006. ISBN 978-1-4020-5370-2.

Joe Alexandersen and Boyan S. Lazarov. Topology optimisation of manufacturable microstructural details without length scale separation using a spectral coarse basis preconditioner. *Computer Methods in Applied Mechanics and Engineering*, 290:156 – 182, 2015. ISSN 0045-7825. doi: https://doi.org/10.1016/j.cma.2015.02.028.

Oded Amir, Niels Aage, and Boyan S. Lazarov. On multigrid-cg for efficient topology optimization. *Structural and Multidisciplinary Optimization*, 49(5):815–829, 2014. ISSN 1615-1488. doi:10.1007/s00158-013-1015-5.

Martin Philip Bendsøe and Noboru Kikuchi. Generating optimal topologies in structural design using a homogenization method. *Computer Methods in Applied Mechanics and Engineering*, 71(2):197 – 224, 1988. ISSN 0045-7825. doi: https://doi.org/10.1016/0045-7825(88)90086-2.

M.P. Bendsoe and O. Sigmund. *Topology Optimization: Theory, Methods, and Applications*. Springer Berlin Heidelberg, 2011. ISBN 9783642076985.

Andrew D. Cramer, Vivien J. Challis, and Anthony P. Roberts. Microstructure interpolation for macroscopic design. *Structural and Multidisciplinary Optimization*, 53(3):489–500, 2016. ISSN 1615-1488. doi:10.1007/s00158-015-1344-7.

Zongliang Du and Hyunsun A. Kim. *Multiscale Design Considering Microstructure Connectivity*. American Institute of Aeronautics and Astronautics, 2018. doi: doi:10.2514/6.2018-1385.

James K. Guest and Jean H. Prévost. Optimizing multifunctional materials: Design of microstructures for maximized stiffness and fluid permeability. *International Journal of Solids and Structures*, 43(22):7028 – 7047, 2006. ISSN 0020-7683. doi: https://doi.org/10.1016/j.ijsolstr.2006.03.001.

J.K. Guest, J. H. Prévost, and T. Belytschko. Achieving minimum length scale in topology optimization using nodal design variables and projection functions. *International Journal for Numerical Methods in Engineering*, 61(2):238–254, 2004. doi:10.1002/nme.1064.

Z. Hashin and S. Shtrikman. A variational approach to the theory of the elastic behaviour of multiphase materials. *Journal of the Mechanics and Physics of Solids*, 11(2):127 – 140, 1963. ISSN 0022-5096. doi:https://doi.org/10.1016/0022-5096(63)90060-7.

B. Hassani and E. Hinton. A review of homogenization and topology optimization i—homogenization theory for media with periodic structure. *Computers and Structures*, 69(6):707 – 717, 1998. ISSN 0045-7949. doi:https://doi.org/10.1016/S0045-7949(98)00131-X.

Helena M. A. Kolken, Shahram Janbaz, Sander M. A. Leeflang, Karel Lietaert, Harrie H. Weinans, and Amir A. Zadpoor. Rationally designed meta-implants: a combination of auxetic and conventional meta-biomaterials. *Mater. Horiz.*, 5:28–35, 2018. doi:10.1039/C7MH00699C.

Boyan S. Lazarov. Topology optimization using multiscale finite element method for high-contrast media. In Ivan Lirkov, Svetozar Margenov, and Jerzy Waśniewski, editors, *Large-Scale Scientific Computing*, pages 339–346. Springer Berlin Heidelberg, Berlin, Heidelberg, 2014. ISBN 978-3-662-43880-0.

Surya N. Patnaik, James D. Guptill, and Berke Laszlo. Merits and limitations of optimality criteria method for structural optimization. *International Journal for Numerical Methods in Engineering*, 38(18):3087–3120, 1995. doi:10.1002/nme.1620381806.

A. Radman, X. Huang, and Y. M. Xie. Topology optimization of functionally graded cellular materials. *Journal of Materials Science*, 48(4):1503–1510, 2013. ISSN 1573-4803. doi:10.1007/s10853-012-6905-1.

H. Rodrigues, J.M. Guedes, and M.P. Bendsoe. Hierarchical optimization of material and structure. *Structural and Multidisciplinary Optimization*, 24(1):1–10, 2002. ISSN 1615-1488. doi:10.1007/s00158-002-0209-z.

Ole Sigmund. Morphology-based black and white filters for topology optimization. *Structural and Multidisciplinary Optimization*, 33(4):401–424, 2007. ISSN 1615-1488. doi:10.1007/s00158-006-0087-x.

Ole Sigmund. Systematic design of metamaterials by topology optimization. In R. Pyrz and J. C. Rauhe, editors, *IUTAM Symposium on Modelling Nanomaterials and Nanosystems*, pages 151–159. Springer Netherlands, Dordrecht, 2009. ISBN 978-1-4020-9557-3.

Ole Sigmund and Kurt Maute. Topology optimization approaches. *Structural and Multidisciplinary Optimization*, 48(6):1031–1055, 2013. ISSN 1615-1488. doi:10.1007/s00158-013-0978-6.

Krister Svanberg. The method of moving asymptotes—a new method for structural optimization. *International Journal for Numerical Methods in Engineering*, 24(2):359–373, 1987. doi:10.1002/nme.1620240207.

Chuang Wang, Ji Hong Zhu, Wei Hong Zhang, Shao Ying Li, and Jie Kong. Concurrent topology optimization design of structures and non-uniform parameterized lattice microstructures. *Structural and Multidisciplinary Optimization*, 58(1):35–50, 2018. ISSN 1615-1488. doi:10.1007/s00158-018-2009-0.

Fengwen Wang, Boyan Stefanov Lazarov, and Ole Sigmund. On projection methods, convergence and robust formulations in topology optimization. *Structural and Multidisciplinary Optimization*, 43(6):767–784, 2011. ISSN 1615-1488. doi:10.1007/s00158-010-0602-y.

J.K. Wessel. *The Handbook of Advanced Materials: Enabling New Designs*. Wiley-Interscience publication. Wiley, 2004. ISBN 9780471465171.

J. Wu, N. Aage, R. Westermann, and O. Sigmund. Infill optimization for additive manufacturing; approaching bone-like porous structures. *IEEE Transactions on Visualization and Computer Graphics*, 24(2):1127–1140, 2018. ISSN 1077-2626. doi:10.1109/TVCG.2017.2655523.

Liang Xia and Piotr Breitkopf. Design of materials using topology optimization and energy-based homogenization approach in matlab. *Structural and Multidisciplinary Optimization*, 52(6):1229–1241, 2015. ISSN 1615-1488. doi:10.1007/s00158-015-1294-0.

Shiwei Zhou and Qing Li. Design of graded two-phase microstructures for tailored elasticity gradients. *Journal of Materials Science*, 43(15):5157, 2008. ISSN 1573-4803. doi:10.1007/s10853-008-2722-y.